Complex-classical mechanism of the tunnelling process in strongly coupled 1.5-dimensional barrier systems

2003 J. Phys. A: Math. Gen. 36 7953

(http://iopscience.iop.org/0305-4470/36/29/305)

INSTITUTE OF PHYSICS PUBLISHING JOURNAL OF PHYSICS A: MATHEMATICAL AND GENERAL

J. Phys. A: Math. Gen. **36** (2003) 7953–7987 PII: S0305-4470(03)55731-6

Complex-classical mechanism of the tunnelling process in strongly coupled 1.5-dimensional barrier systems

Kin'ya Takahashi[1,2,4] **and Kensuke S Ikeda**[3]

[1] The Physics Laboratories, Kyushu Institute of Technology, Kawazu 680-4, Iizuka 820-8502, Japan
[2] CEA-Service de Physique Theorique de Saclay, F-91191 Gif-sur-Yvette Cedex, France
[3] Department of Physical Sciences, Faculty of Science and Engineering, Ritsumeikan University, Noji-higashi 1-1-1, Kusatsu 525-0055, Japan

Received 30 October 2002, in final form 10 June 2003
Published 8 July 2003
Online at stacks.iop.org/JPhysA/36/7953

Abstract

The fringed tunnelling, which can be observed in strongly coupled 1.5-dimensional barrier systems as well as in autonomous two-dimensional barrier systems, is a manifestation of intrinsic multi-dimensional effects in the tunnelling process. In this paper, we investigate such an intrinsic multi-dimensional effect on the tunnelling by means of classical dynamical theory and semiclassical theory, which are extended to the complex domain. In particular, we clarify the underlying *classical* mechanism which enables multiple tunnelling trajectories to simultaneously contribute to the wavefunction, thereby resulting in the formation of the remarkable interference fringe on it. Theoretical analyses are carried out in the low-frequency regime based upon a complexified adiabatic tunnelling solution, together with the Melnikov method extended to the complex domain. These analyses reveal that the fringed tunnelling is a result of a *heteroclinic-like entanglement* between the complexified stable manifold of the barrier-top unstable periodic orbit and the incident beam set. Tunnelling particles reach the real phase plane very promptly, guided by the complexified stable manifold, which gives quite a different picture of the tunnelling from the ordinary instanton mechanism. More fundamentally, the entanglement is attributed to a *divergent movement* of movable singularities of the classical trajectory, namely, to a singular dependence of singularities on its initial condition.

PACS numbers: 05.45.Mt, 03.65.Xp, 03.65.Sq, 05.45.−a

[4] Present address: The Physics Laboratories, Kyushu Institute of Technology, Kawazu 680-4, Iizuka 820-8502, Japan.

1. Introduction

Tunnelling phenomena are intrinsic quantum effects having no classical counterpart. By the definition of the tunnelling effect, no classical trajectory is responsible for the tunnelling phenomenon and it cannot be described only in terms of classical mechanics. However, it is known that some aspects of tunnelling phenomena can be described on the basis of semiclassical theory if we are allowed to use classical trajectories continued to the complex domain [1]. The complexified classical trajectories indeed play a key role in the semiclassical description of tunnelling phenomena, which is beyond the reach of the real-domain semiclassical theory. In particular, the complex-domain semiclassical theory, e.g. complex WKB, instanton theory and so on [2], has successfully been applied to the tunnelling problems of one-dimensional (1D) systems and effectively 1D systems including (classically) integrable and nearly integrable systems of multi-dimensions [3, 4]. Furthermore, it is known that, in the 1D case, even the exact quantum theory may be recovered by the resummation of the semiclassical expansion [5, 6].

On the other hand, the semiclassical theory of multi-dimensional tunnelling phenomena [7–9] is a long-standing problem which seems to be far from completion. Even if we restrict ourselves to the real domain, the existence of chaotic behaviour in classically non-integrable multi-dimensional systems is a real obstacle to endowing semiclassical theory with a rigorously mathematical basis, while it is known that some practical applications of semiclassical theory work well in predicting quantal quantities which are used to characterize the quantum chaotic nature of a system under consideration [10, 11]. The extension of the phase space to the complex domain will introduce further complexities and difficulties. Moreover, very little is known about the complexified chaotic dynamics of systems of more than one dimension.

In the last decade, the manifestation of chaos in multi-dimensional tunnelling phenomena has attracted much attention [12–14], and there have been some successful attempts to apply the (complex-domain) semiclassical theory to multi-dimensional tunnelling in classically non-integrable systems [15–17]. In particular, it has been demonstrated that the semiclassical theory using the complexified classical trajectories can well reproduce the complicated features of the tunnelling wavefunction [16, 17].

Furthermore, it has been suggested that there are some profound relationships between the tunnelling problem and some key concepts of complex dynamical systems, such as Julia sets, Böttcher coordinates and so on [18]. However, these semiclassical studies have been successfully made for a particular class of system operated at *discretized* times, i.e. quantum maps. As for the tunnelling problem of ordinary multi-dimensional systems evolved in time by the *continuous* time Schrödinger equation, it is still very unclear how the tunnelling process is influenced by the multi-dimensionality and the underlying chaotic dynamics, although some efforts have been made on the basis of the trace-formula formalism [15].

In previous papers [19–22], we have demonstrated that a new class of barrier tunnelling phenomena may be observed in 1.5-dimensional (1.5D) systems (i.e. periodically driven 1D systems). The tunnelling component, which is described by the standard instanton theory (or its modified version) in the weak perturbation regime, becomes accompanied by a remarkable fringe pattern as the perturbation strength exceeds a certain characteristic value.

It is easily shown that periodically perturbed 1D systems can be regarded as a specific class of two-dimensional (2D) systems [23]. Such a fictitious 2D system can well mimic both classical and quantum dynamics of an intrinsic 2D autonomous system which has a harmonic channel that plays the role of the periodic perturbation in the 1.5D system. Indeed, a similar fringed pattern on the tunnelling component is also observed for the corresponding intrinsic 2D autonomous system [21, 22, 24] and it is conjectured that the emergence of fringed patterns

is a common feature characterizing the tunnelling phenomena of multi-dimensional barrier systems.

Based upon the complex-domain semiclassical theory, we have also shown that such a fringe is brought about by the interference among the multiple tunnelling trajectories, which are never predicted by the 1D approach such as instanton theory [20–22]. Furthermore, we have succeeded in elucidating the underlying classical mechanisms which rule the tunnelling trajectories contributing to the fringed tunnelling, and its essence has been sketched in preliminary reports [21, 22]. It turns out that the phenomenon is a result of a complexified *heteroclinic-like entanglement*. Surprisingly enough, such an entanglement is a manifestation of *divergent movement* of the movable singularities of the complexified classical trajectory.

Note that the existence of movable singularities of the complexified classical trajectory for non-linear systems is well known in the field of the Painlevé analysis, and the analysis of movable singularities not only plays a key role in the judgement of integrability of a given system [25], but also, if it is not integrable, provides further information on the nature of chaotic motion inherent in the system [25, 26]. However, we do not know of any report on the relationship between the entanglement of complexified invariant manifolds and the singular behaviour of singularities.

The aim of this paper is to investigate in detail the underlying mechanism of fringed tunnelling on the basis of the complex-domain semiclassical theory. We are particularly concerned with the hidden *classical* origin of the simultaneous contribution of multiple complexified tunnelling trajectories, which is directly reflected in the formation of the interference fringe on the tunnelling wavefunction; how the tunnelling trajectories are influenced by the divergent movement of the singularities together with the *heteroclinic-like entanglement* between the complexified invariant sets. As a result, we will provide a comprehensive explanation to understand the fringed tunnelling in terms of complexified classical trajectories.

Our tunnelling model of 1.5D systems is considered as a minimal model of multi-dimensional barrier scattering systems which can be formulated by using the standard tools of scattering theory, such as the wave-operator and/or S-matrix [27]. Indeed, the appearance of such a heteroclinic-like entanglement in the complex domain seems to be quite common for multi-dimensional systems. Thus, the classical mechanism, which will be clarified in the following, can provide a clue to understanding how the complex classical trajectories contributing to complicated multi-dimensional tunnelling phenomena are influenced in general by dynamical objects peculiar to the multi-dimensional complexified phase space.

This paper is organized as follows. We first introduce, in section 2, the wave-matrix of periodically perturbed systems, and a semiclassical expression for the wave-matrix is derived by applying the saddle-point approximation. We introduce basic tools for the representation of classical trajectories contributing to the semiclassical wave-matrix: one is the $\mathcal{M}$-set, which is the set of initial conditions of the contributing trajectories, and the other is the $\mathcal{L}$-set representing the Lagrangian manifold of the contributing trajectories. Important remarks on the Stokes phenomenon and on movable singularities of the complexified trajectory, which are peculiar to the complex-domain semiclassics, are also discussed in connection with the particular choice of the potential function. The periodically perturbed Eckart potential is used in this paper.

In section 3 we discuss the nature of classical tunnelling trajectories in the simplest situation of the unperturbed Eckart barrier, and we show that the (movable) singularities of the classical solution control the asymptotic nature of trajectories, which are integrated along topologically different integration paths with respect to singularities, namely, the reflected

trajectory and the transmitted (i.e. tunnelling) trajectory. The *critical point* is introduced as the particular initial point at which the singularities diverge. At the critical point, a discontinuous transition occurs in the asymptotic nature of the complexified trajectory.

In section 4 we return to the periodically perturbed Eckart system. Numerically our complex-domain semiclassical theory works extremely well and can reproduce every detail of the complicated fringed tunnelling wavefunction. Based on the success, we numerically elucidate the mechanism of the fringed tunnelling. Numerical evidence exhibiting the presence of critical points on the complex initial time plane is given, and it is further shown that a particular set $\mathcal{M}_c$ of initial conditions, which is a subset of $\mathcal{M}$, always exists very close to the critical point. With these numerical observations we describe how multiple tunnelling trajectories contribute simultaneously to the semiclassical wave-matrix, thereby inducing the remarkable interference pattern on the tunnelling wavefunction.

In section 5, we summarize the numerically observed results discussed in section 4, and perform theoretical analyses to clarify the underlying classical mechanism of the numerical observations. The analyses are carried out in the low-frequency regime by using an adiabatic classical solution together with the Melnikov method extended to the complex domain. It is first shown that the critical point corresponds to the intersection between the complexified stable manifold (CSM) of the unstable periodic orbit on the top of the potential barrier and the incident beam set decided by the incident condition. It is shown that the adiabatic solution guarantees that the set $\mathcal{M}_c$ exists very close to the critical point and the singularities of the trajectory starting at the critical point diverge logarithmically. The theoretical analyses succeed in proving all the numerical observations, and the mechanism of the fringed tunnelling is described theoretically. It is concluded that the fringed tunnelling is a manifestation of a *heteroclinic-like entanglement* between the CSM and the incident beam set. The condition for the fringed tunnelling to occur is also presented.

Section 6 is devoted to the summary and a discussion of the results obtained in this paper and prospects for the future works subsequent to this paper.

2. Semiclassical wave-matrix

In our recent publications [19, 28], we formulated the scattering problem for periodically perturbed systems by introducing a time-dependent analogue of the scattering eigenstate (i.e. wave-matrix) and obtained a semiclassical expression for it. In this section, we describe the outline of our formula.

2.1. Wave-matrix for periodically perturbed systems

The model system that we consider in this paper is of a periodically perturbed spatially localized potential, whose Hamiltonian is represented as

$$\begin{aligned} H(Q, \hat{P}, \omega t) &= \frac{1}{2M}\hat{P}^2 + V(Q, \omega t) \\ &= \frac{1}{2M}\hat{P}^2 + V_0(Q) + \epsilon v(Q, \omega t) \qquad (M = 1) \end{aligned} \tag{2.1}$$

where Q is the coordinate and $\hat{P} = -\mathrm{i}\hbar\frac{\partial}{\partial Q}$ is the momentum operator. The potentials $V_0(Q)$ and $v(Q, \omega t)$ are both localized around $Q = 0$ and decay promptly as $\lim_{Q\to\pm\infty} V(Q) \to 0$ and $\lim_{Q\to\pm\infty} v(Q, t) \to 0$, where V_0 denotes the unperturbed potential independent of time, and v is a periodic function of time, i.e. $v(Q, \omega t + 2\pi) = v(Q, \omega t)$. Suppose that the incident plane wave comes from the right-hand side at a constant momentum P_1. If

$|P_1|$ is sufficiently small, the quantum probability observed in the transmissive side is due to the tunnelling effect. For such an incident condition, we can obtain a quasi-eigenstate as a stationary solution, i.e. Floquet solution [19],

$$\Psi_{P_1}(Q_2, t_2) = \mathrm{e}^{-\mathrm{i}E_1 t_2/\hbar}\langle Q_2|\hat{\Omega}_1^+(\omega t_2)|P_1\rangle \tag{2.2}$$

where t_2 and Q_2 are the observatory time and coordinate, respectively, and $\langle Q_2|\hat{\Omega}_1^+(\omega t_2)|P_1\rangle$ is the periodic part of Floquet solution which varies periodically being tuned to the periodic perturbation.

The periodic stationary solution $\langle Q_2|\hat{\Omega}_1^+(\omega t_2)|P_1\rangle$ is the wave-matrix for periodically perturbed systems, i.e. the 1D time-dependent analogue of the wave-operator [19]. A convenient representation of the wave-operator $\hat{\Omega}_1^+$ (the wave-matrix) is obtained as follows [19]

$$\langle Q_2|\hat{\Omega}_1^+(\omega t_2)|P_1\rangle = \lim_{|Q_1|\to\infty}\sqrt{\frac{|P_1|}{2\pi\hbar}}\,\mathrm{e}^{\mathrm{i}P_1Q_1/\hbar}\int_0^\infty \mathrm{d}s\,\langle Q_2|\hat{U}(\omega t_2 : \omega t_2 - \omega s)|Q_1\rangle \exp\left\{\mathrm{i}\frac{E_1 s}{\hbar}\right\} \tag{2.3}$$

where $\hat{U}$ denotes the time propagator of the system defined by

$$\hat{U}(\theta + \omega t : \theta) = \mathcal{T}\exp\left\{-\frac{\mathrm{i}}{\hbar}\int_0^t \mathrm{d}s\,\hat{H}(\theta + \omega s)\right\} \qquad (\mathcal{T}\text{: time ordering operator}). \tag{2.4}$$

Then, the wave-operator is nothing more than the time-dependent analogue of the energy-domain Green function.

2.2. Semiclassical formulation of wave-matrix and complex classical trajectories

Applying the saddle-point approximation to the 1D time-dependent wave-matrix given by equation (2.3), we can obtain the semiclassical expression for the wave-matrix [19]

$$\langle Q_2|\hat{\Omega}_1^+(t_2)|P_1\rangle \sim \sum_{\text{c.t.}}\lim_{Q_1\to\infty}\sqrt{\frac{|P_1|}{2\pi\hbar}}\,\mathrm{e}^{\mathrm{i}P_1Q_1/\hbar}\left[\frac{1}{P_1}\frac{\partial^2 S_\Omega}{\partial E_1\partial Q_2}\right]^{1/2}\exp\left\{\frac{\mathrm{i}}{\hbar}S_\Omega(Q_2, t_2, Q_1, E_1)\right\} \tag{2.5}$$

where the classical action S_Ω is defined by

$$S_\Omega(Q_2, t_2, Q_1, E_1) \equiv \int_{t_1}^{t_2}[P(t)^2/2 - V(Q, \omega t)]\,\mathrm{d}t + E_1(t_2 - t_1) \tag{2.6}$$

which is the function of the initial coordinate Q_1, initial energy E_1, arrival time t_2, and arrival coordinate Q_2. Note that the initial time t_1 is not an independent variable but $t_1 = t_1(Q_2, t_2, Q_1, E_1)$.

To describe the tunnelling probability by the semiclassical theory, we should take the classical trajectories travelling in the complex domain of the phase space, with the classical equation of motion

$$\mathrm{d}^2Q/\mathrm{d}t^2 = -\partial V(Q, \omega t)/\partial Q. \tag{2.7}$$

The initial and final sets of dynamical variables deciding the classical action, namely (Q_1, E_1) and (Q_2, t_2) in our case, are the observables specifying the initial and final quantum states to which real numbers should be assigned. Since t_1 is regarded as being canonically conjugate to E_1 and cannot be observed quantum mechanically, we can choose any complex number for it, and the lapse time $s = t_2 - t_1$ may take a complex value [19]. To the best of our knowledge, legitimate prescription for complexifying canonically paired observables was first presented by Miller [8].

To decide contributing classical trajectories satisfying the fixed boundary condition mentioned above, the initial time t_1 is taken as a complex search parameter. In other words, we should solve a shooting problem; for a relevant choice of the initial time, the trajectory hits the target Q_2 at t_2 and otherwise it misses. In order to obtain the quantum probability as a function of the coordinate, the end coordinate $Q_2 = Q(t_2 - t_1, t_1, P_1, Q_1)$ is scanned along the real line with fixed $t_2 \in \mathbf{R}$, then the search parameter t_1 will trace 1D curve(s) on the complex plane.

The 1D set composed of such curves on the complex t_1 plane is called $\mathcal{M}$-set according to Shudo and Ikeda [16], which is defined by [19]

$$\mathcal{M} = ((\xi, \eta) \in \mathbf{R}^2 | \mathrm{Im}\{Q(t_2 - (\xi + \mathrm{i}\eta), \xi + \mathrm{i}\eta, P_1, Q_1)\} = 0) \qquad \text{where} \quad \xi + \mathrm{i}\eta \equiv t_1. \tag{2.8}$$

The set $\mathcal{M}$ is in general composed of disconnected curves and we call each piece of the disconnected components the complex branch. A single branch is not always enough to reconstruct the quantum probability, but two or more branches and sometimes an infinite number of branches may simultaneously contribute to it, as will be shown later. The $\mathcal{M}$-set enables us to visualize the structure of the set of initial conditions of contributing trajectories on the search plane.

We also introduce the $\mathcal{L}$-set [19]

$$\mathcal{L} = ((Q_2, P_2) | Q_2 = Q(t_2 - t_1, t_1, P_1, Q_1), P_2 = P(t_2 - t_1, t_1, P_1, Q_1), t_1 \in \mathcal{M}) \tag{2.9}$$

which is the Lagrangian manifold, namely, the set of end points (Q_2, P_2) of the trajectories at the given time t_2 starting from the initial condition in the $\mathcal{M}$-set.

There are two particular problems peculiar to the complex-domain semiclassical theory, which introduce some difficulties in the practical construction of the semiclassical wave-matrix. One is the Stokes phenomenon [29, 30]. The classical trajectories which satisfy the boundary condition of the wave-matrix do not always contribute to the semiclassical formula. Indeed, each complexified trajectory in general has a complex conjugate partner, then $\mathrm{Im}\, S_\Omega(Q_2, t_2, Q_1, E_1)$ of one of the paired trajectories has a negative sign and the exponential factor $\mathrm{e}^{\mathrm{i}S_\Omega/\hbar}$ in equation (2.5) diverges in the semiclassical limit of $\hbar \to 0$. Such trajectories obviously make an unphysical contribution, and they must be removed. Removal of the unphysical trajectories is carried out by a proper treatment based upon the principle of exponential dominance [29–32] together with the tree pruning hypothesis proposed by Shudo and Ikeda [32].

The other problem is that the complexified trajectory in general has singularities unless the potential is harmonic and, moreover, if they exist, they in general move with the initial condition (*movable singularities*) [25]. Even in the 1D static barrier problem ($\epsilon = 0$), the contributing complex classical trajectory has singularities and they play a key role in the description of the barrier tunnelling phenomenon from a semiclassical point of view, which can be demonstrated rather in detail by the following physical argument.

The quantum scattering eigenfunction has both transmitted and reflected components, which respectively converge to the plane waves with the constant momenta of opposite signs in the asymptotic limits (i.e. $Q \to -\infty$ or $Q \to \infty$). In order that such a feature is describable by the semiclassical theory, the (complexified) classical trajectory should not be unique even though it starts from a given initial condition, and should bifurcate into at least two sorts of trajectories, namely, transmitted and reflected. This should be, in principle, possible by properly taking different integration paths, say C and C', on the complexified time plane from the same origin. C and C' are chosen in such a way that the integration of the classical equation of motion along the two paths may yield two trajectories travelling in the two opposite

asymptotic regions (i.e. $Q \to -\infty$ or $Q \to \infty$) in the limit of $\mathrm{Re}\, t = \mathrm{Re}\, t' \to +\infty$, where t and t' are the two ends of C and C', respectively. Since the motion is free from any force at t, the trajectory ending at t should be continued analytically to that at t' along a shortcut connecting t and t', keeping the momentum at the same value. It is, however, impossible because the momenta have opposite signs at t and t', which means that there exists a singularity (or singularities) in the region between C and C'.

The presence of singularities results into the multiple-valuedness of the trajectory [19, 20], which creates further complication in the shooting problem as to the topology of the integration path going among the singularities under the constraint of the boundary condition. A more important problem is that the movable singularities often move very sensitively against a slight change of the initial condition. Such a sensitive movement may change the topology of the integration path around the singularities, thereby making the nature of the trajectory along the integration path change drastically. Indeed, as will be elaborated in what follows, this is the main subject of this paper.

In the actual calculation in this paper, we take a particular form of the potential well known as the Eckart potential:

$$V_0(Q) = \mathrm{sech}^2(Q) \qquad v(Q, \omega t) = \sin(\omega t)\,\mathrm{sech}^2(Q). \tag{2.10}$$

The Eckart potential has well-defined asymptotic regions due to its exponential decay, and its quantum mechanics can be solved exactly. Above all, it gives an expression of the branched trajectories in terms of elementary functions in the unperturbed limit. This is the very reason why we choose the perturbed Eckart potential as the 'minimal' model[5].

3. Static barrier

First of all, we would like to discuss the crucial role of singularities (branch points) of the classical trajectory for the static Eckart barrier problem [33].

3.1. A classical solution of the static barrier

In the limit of $\epsilon = 0$, the classical equation of motion can be easily integrated, and if the incident energy E_1 is less than the potential barrier, i.e. $0 < E_1 < 1$, we can immediately obtain the following solution

$$Q(t - t_1, Q_1, P_1) = \sinh^{-1}(\lambda \cosh(\sqrt{2E_1}(t - t_0))) \tag{3.1}$$

for the incident condition, $Q = Q_1 \gg 1$, $P = P_1 < 0$ at $t = t_1$, where the parameter λ is defined by

$$\lambda \equiv \sqrt{1/E_1 - 1}. \tag{3.2}$$

If $0 < E_1 < 1$, λ takes a positive real value, while if E_1 exceeds unity (i.e. above the potential barrier), it takes a pure imaginary value, and no classical trajectories can go through the potential barrier for $0 < E_1 < 1$.

At $t = t_0$ the trajectory hits the turning point given by

$$Q_{\mathrm{turn}} = Q(t_0 - t_1) = \log\left[\lambda + \sqrt{\lambda^2 + 1}\right]. \tag{3.3}$$

[5] The inverted quadratic potential $V_0 = -Q^2/2$ can be taken as an example of a solvable barrier potential, but it has no asymptotic regions in which the particle moves freely, and the associated singularities sit in the infinity.

The lapse time $t_0 - t_1$, which is the time for the trajectory to spend until the turning point, is represented by

$$t_0 - t_1 = (Q_1 - \log\lambda)/\sqrt{2E_1} \equiv t_{01}. \tag{3.4}$$

3.2. Singularities and integration paths of classical trajectories

From the solution of the coordinate Q in equation (3.1), we can easily find that the trajectory has a branch point as a singularity at the time t_{sg} which is given by the relation, $\cosh(\sqrt{2E_1}(t_{sg} - t_0)) = \pm i/\lambda$. In terms of the lapse time $s = t - t_1$, the location of singularities is given by

$$Sg_n^{\pm} = (Q_1 - \log\lambda \pm \sinh^{-1}(1/\lambda))/\sqrt{2E_1} + i(-n + 1/2)\Delta t_I/2 \tag{3.5}$$

where Δt_I is defined by $\Delta t_I \equiv 2\pi/\sqrt{2E_1}$. Note that the singularity $Sg_n^{\pm}$ is just the lapse time at which $Q_{sg} = i\pi(m + 1/2)$, where the potential V_0 diverges. It can easily be checked that the branch point of the type $\left(s - Sg_n^{\pm}\right)^{1/2}$ appears when the trajectory hits $Q = Q_{sg}$, because the classical equation of motion is asymptotically given by $d^2Q/dt^2 \propto (Q - Q_{sg})^{-3}$ close to Q_{sg}. Also note that, if the initial position Q_1 and momentum P_1 are fixed, the singularities on the s-plane are independent of t_1, because of the time-translational symmetry in autonomous systems.

Let us see the location of the singularities (see figure 1(*a*)). Sg_n^- and Sg_n^+ are located periodically with the interval $\Delta t_I/2$ on two different lines parallel to the Im{s}-axis, respectively. The interval of the two lines, i.e. the distance between Sg_n^+ and Sg_n^-, is decided by $\frac{2}{\sqrt{2E_1}}\sinh^{-1}(1/\lambda)$, namely it is a function of E_1. The point t_{01} is located on the real axis and is a middle point between the two lines.

In figure 1(*a*), we also see how the physically significant integration paths go among the singularities in topologically different ways. In practical calculations, we can take a path homotopic to one of such representative integration paths C_n. The two figures in figure 1(*b*) depict complex trajectories $(Q(t), P(t))$ for cases of $E_1 < 1$ and $E_1 > 1$, which are obtained along various integration paths in figure 1(*a*). Each path C_n defines a branch of the solution and the trajectory integrated along C_n reaches the reflective or transmissive region passing through the scattering region. Note that, if the end point of the integration path is taken in the region $\left(\mathrm{Re}\, Sg_n^- < \mathrm{Re}\, s (= \mathrm{Re}(t_2 - t_1)) < \mathrm{Re}\, Sg_n^+\right)$, then the trajectory reaches the scattering region.

In the case of E_1 less than the barrier height, the trajectory starting at the initial point (Q_1, P_1) hits the classical turning point at $s = t_{01}$, and after t_{01}, it rotates along a complex elliptic orbit in the classically forbidden region of the potential barrier. Such a complex bouncing trajectory is often called an instanton. After rotating along it $n/2$ times, the trajectory is reflected back (to $Q = +\infty$) for an even number integration path, and tunnels toward $Q = -\infty$ for an odd number n.

Therefore, the periodicity of the singularities in the imaginary direction is attributed to the periodicity of the complex elliptic orbit, and the existence of such singularities results in an infinite number of branches of the Riemann sheet on the lapse time plane, half of which contribute to the reflection and the other half of which yield transmitted components. Since the presence of the complex elliptic orbit is common to 1D scattering barriers, then the basic geometrical structure of the Riemann sheet obtained above with respect to the tunnelling integration paths C_n is not the specific feature of the Eckart barrier, but generic for 1D scattering barriers as discussed in section 2. The destination of the trajectory, i.e. which is

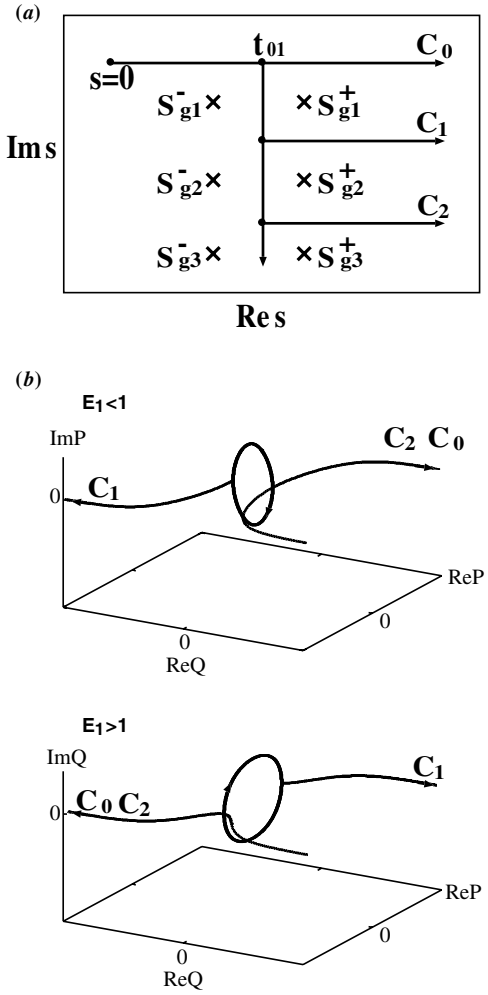

Figure 1. Relation between the integration paths and the complexified trajectories of the unperturbed barrier system. (*a*) Singularities and representative integration paths on the lapse time plane. (*b*) Complex trajectories obtained along various integration paths depicted in (*a*). The cases of $E_1 < 1$ and of $E_1 > 1$ are shown.

either the transmissive side or the reflective side, changes depending on a choice of integration paths.

It should be noted that all the trajectories with odd integration paths contribute to the tunnelling component[6], but the major contribution to it comes from the trajectory with C_1, because more round trips along the complex ellipse result in a larger imaginary part of the classical action. Thereby, contributions of the other integration paths C_{2n-1} $(n > 1)$ are extremely small and negligible.

[6] When including contribution from trajectories integrated along higher-order integration paths C_n $(n > 1)$, we have to take some care to determine their Stokes coefficients. For a practical treatment of the static barrier case, see, for example, [34].

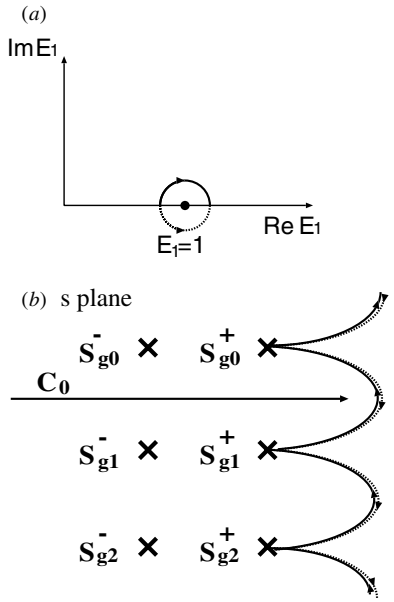

Figure 2. Critical point and movement of the singularities Sg_n^+ associated with it for the unperturbed barrier system. (*a*) Critical point at $E_1 = 1$ on the complexified energy plane. Two paths are denoted by solid and dashed lines going halfway around it in different directions. (*b*) Movement of the singularities Sg_n^+ together with the integration path C_0 is shown on the lapse time plane as E_1 moving along the paths in (*a*).

If the parameter λ is allowed to take a pure imaginary value, $\lambda = \pm i|\lambda| = \pm i\sqrt{1 - 1/E_1}$, the solution for the case $E_1 > 1$ is also obtained. Then, the location of the singularities on the *s*-plane is estimated as follows:

$$Sg_n^{\pm} = (Q_1 - \log|\lambda| \pm \cosh^{-1}(1/|\lambda|))/\sqrt{2E_1} + i(-n + 1/2)\Delta t_I/2 \mp i\Delta t_I/2. \tag{3.6}$$

At first glance, the singularities are located in the same way as the case of $E_1 < 1$, but the nature of the solution is different. That is, the reflective and transmissive branches exchange. In the case of $E_1 < 1$, if we take, for example, the integration path C_0, then we obtain the solution arriving at a point in the reflective region. On the other hand, in the case of $E_1 > 1$, the solution reaches the transmissive side for the same integration path (see the bottom figure in figure 1(*b*)). For a path C_n, after $n/2$ times rotations in the classically forbidden region, the trajectory goes to $Q = -\infty$ for even n and is reflected back to $Q = +\infty$ for odd n.

Such a discontinuous change is attributed to the singular behaviour of the singularities Sg_n^+ as E_1 goes across 1. This is more comprehensible by analytically continuing the real energy E_1 to the complex plane. From equation (3.5), Sg_n^+ is evaluated around E_1 as

$$Sg_n^+ \sim \frac{1}{2E_1}(-\log\{1 - E_1\} + \text{const} + \text{small corrections}). \tag{3.7}$$

For the integration path with a finite lapse time ($s = t_2 - t_1$) such as C_0, there exists a path of E_1 which goes halfway, clockwise or anticlockwise, around the point $E_1 = 1$, keeping the distance from it short enough (see figure 2(*a*)), so that with movement of E_1 along the path, all Sg_n^+ can go far away from the origin and return to the original sites avoiding the integration path, shifting by $\pm\Delta t_I/2$ in the direction of the imaginary axis. (The sign depends on a choice of paths; see figure 2(*b*).) This fact means that the reflective and transmissive

branches exchange, and the destination of the trajectory along the path changes abruptly but continuously from the reflective side to the transmission side in the case of C_0.

Let us regard the movable singularity as a function of the initial condition(s). We call the particular initial value at which all or a part of the singularities exhibit singular behaviour the *critical point*. In short, the critical point is the singular point of the movable singularities.

It is worth mentioning the trajectory launched from the critical initial condition. In the limit of $E_1 \to 1$, the positions of the two types of singularity are, respectively, given by

$$Sg_n^- \to Q_1/\sqrt{2} - \log 2/\sqrt{2} + \mathrm{i}(-n + 1/2)\Delta t_I/2 \tag{3.8}$$

$$Sg_n^+ \sim Q_1/\sqrt{2} + \log(2/\lambda^2)/\sqrt{2} + \mathrm{i}(-n + 1/2)\Delta t_I/2 \to \infty. \tag{3.9}$$

Thus, the singularities Sg_n^- remain at finite position, and only Sg_n^+ diverge. The point t_{01} which is the lapse time spent until the turning point also diverges at $E_1 = 1$:

$$t_{01} = t_0 - t_1 = (Q_1 - \log\lambda)/\sqrt{2} \to \infty. \tag{3.10}$$

These divergences are the reflection that the trajectory is on the stable manifold of the unstable fixed point at the origin. The trajectory on the stable manifold is represented by

$$Q(t - t_1, Q_1, P_1) = \sinh^{-1}(\mathrm{e}^{-\sqrt{2}(t-\mu)}) \tag{3.11}$$

where μ is a parameter defined by the initial condition, i.e.

$$\mu \equiv t_1 + (Q_1 - \log 2)/\sqrt{2}. \tag{3.12}$$

The critical point emerges also in the periodically perturbed problem and the above-discussed features around it play a key role in understanding the characteristic tunnelling phenomenon in the strong perturbation regime. This is the main subject in the following arguments.

4. Critical point and fringed tunnelling

On the basis of the arguments in the previous section together with simple intuitive consideration, we predict that the critical point always emerges on the t_1-plane of the periodically perturbed system. We also show some numerical evidence that the critical point drastically influences the nature of tunnelling trajectories and causes the fringed tunnelling in the strong perturbation regime.

4.1. Effects of the periodic perturbation

In the case of the 1D unperturbed tunnelling problem, the movable singularity is the function of E_1 alone, if the initial coordinate Q_1 is chosen in the asymptotic region, and so, given the incident beam set, E_1 is decided and there is no fear that the singularity moves.

However, in 1.5-degrees-of-freedom systems, besides E_1 and Q_1, t_1 is an additional element of the initial condition. Given the incident beam set, the movement of t_1 on the **C**-plane as the search parameter causes the movement of the movable singularity on the lapse time plane, which may become singular at a particular $t_1 = t_{1c}$, namely a manifestation of the critical point.

Indeed, by simple physical consideration we can point out that the emergence of the critical point is quite natural. Here we suppose that ω is so small that the perturbation does not change significantly in the time scale of the particle passing through the scattering region. Taking $t_1 \in \mathbf{C}$ and setting the integration path such as C_0 from t_1, then the time t_h at which the particle reaches the scattering region is the function of t_1 alone and is roughly estimated by

$$t_h(t_1) \sim t_1 + Q_1/|P_1|. \tag{4.1}$$

On the other hand, the potential barrier height at $t = t_h$ is given by

$$V(Q = 0, \omega t_h) = (1 + \epsilon \sin \omega t_h). \tag{4.2}$$

Since t_h has an imaginary part, the amplitude of the perturbation seems as if it is amplified as $\epsilon \to \epsilon\, \mathrm{e}^{\omega|\mathrm{Im}\, t_h|}$, and the lower bound of its oscillation is reduced to $1 - \epsilon\, \mathrm{e}^{\omega|\mathrm{Im}\, t_h|}$. Therefore, even when ϵ is small enough and E_1 is much less than 1, which means that the particle cannot go through the potential by the real classical trajectory, it is possible for the relation

$$E_1 = V(Q = 0, \omega t_h(t_1)) \tag{4.3}$$

to be satisfied by a particular choice of t_1, if $|\mathrm{Im}\, t_1|$ is taken to be sufficiently large. Since we suppose the low-frequency limit of the perturbation, the potential is constant when the particle passes through the scattering region, and our problem is reduced to the 1D tunnelling problem discussed in the previous section. The condition (4.3) is nothing more than the critical condition that the incident energy is equal to the barrier height, and the particular point t_1 that satisfies the condition (4.3) can be regarded as the 'critical point' t_{1c}. From the periodicity of the perturbation, critical points appear periodically on the t_1-plane. As discussed in section 3.2, the nature of the trajectory $t_1 \sim t_{1c}$ may change drastically, if t_1 is traced close to t_{1c}.

If either E_1 is much less than 1, i.e. the unperturbed potential height, and/or the perturbation strength is small enough, the imaginary depth of the 'critical point' t_{1c} that satisfies the condition (4.3) will be so large that t_{1c} will be far from the initial times of major reflected and transmitted trajectories which are calculated along the major integration paths C_0 and C_1, respectively. In such a case, the presence of the critical point does not effectively influence the quantum mechanical behaviour of the system. Such is a situation in the weak perturbation regime, in which the perturbation expansion approach based on the instanton works excellently well [20].

However, if E_1 is near 1 or ϵ is large enough, then the critical point moves toward the real axis and may drastically disturb the original nature of the trajectories defined along the major integration paths. Such is a typical situation generically observed in the strong perturbation regime.

4.2. Numerical example of the critical point

In practice, it is found numerically that such a particular initial time t_{1c}, i.e. the critical point, is always found in the initial time plane t_1 independent of the strength of the perturbation ϵ, although the imaginary depth of t_{1c} changes with ϵ, namely t_{1c} moves down to the real axis with increase of ϵ. Just as expected above, when ϵ exceeds a certain value ϵ_c, t_{1c} affects the major contributing tunnelling trajectories with the integration path C_1. It is in just such a regime that the fringed patterns on the tunnelling component are observed. When the observatory time t_2 is fixed, we can decide the set of the initial points of the trajectories which satisfy the boundary condition of the semiclassical wave-matrix, i.e. the $\mathcal{M}$-set. Concerning the $\mathcal{M}$-set, there exists a remarkable fact that the critical point t_{1c} is always accompanied by a characteristic part of the branch passing very close to it, say $\mathcal{M}_c$, which plays an important role in the construction of the fringed wave pattern on the tunnelling component with the semiclassical formula.

Let us see a typical numerical example, which is obtained in the strong perturbation regime ($\epsilon = 0.2$, $\omega = 0.3$ and $E_1 = 0.75$). Here we do not show the whole $\mathcal{M}$-set (see the next subsection), but a magnified picture of $\mathcal{M}$-set near a certain critical point in figure 3(*a*). As stated above, we can find $\mathcal{M}_c$ running very close to the critical point t_{1c}. Figure 3(*b*) shows the movement of singularities on the lapse time plane together with the integration path C_1. When the initial time t_1 is at point 1 in figure 3(*a*), the topology of

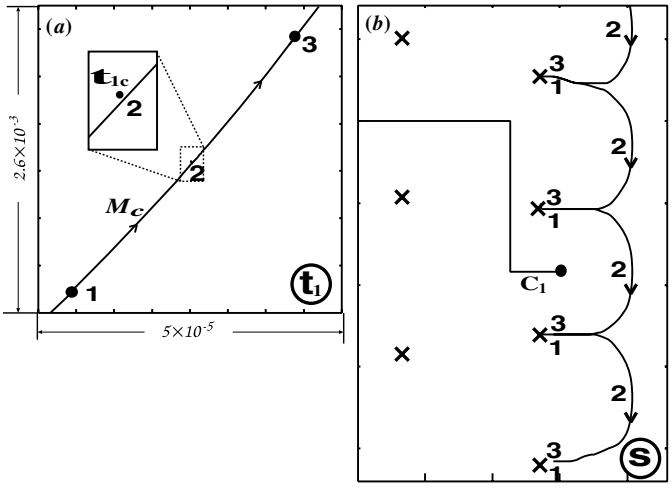

Figure 3. Switching of the path topology induced by the divergence movement of the singularities Sg_n^+ at a critical point under a strong perturbation. The parameters are set as follows: $\epsilon = 0.2$, $E_1 = 0.75$, $\omega = 0.3$, $\hbar = 1000/(3\pi \times 2^{10}) \sim 0.1036$, and $\omega t_2 = 0 (\mathrm{mod}\, 2\pi)$. (*a*) Magnified picture of the vicinity of the critical point t_{1c}, which corresponds to the first critical point in figure 4(*a*). The characteristic subset $\mathcal{M}_c$ (the branch **1** in figure 4(*a*)) exists passing close to the critical point t_{1c}. (*b*) The singularities Sg_n^+ move detouring the integration path C_1 on the lapse time plane, when t_1 varies as $1 \rightarrow 2 \rightarrow 3$ along $\mathcal{M}_c$ on the t_1- plane in (*a*).

the integration path is essentially the same as the case of $E_1 < 1$ in the static limit, and the trajectory reaches the transmissive side at $t = t_2$. Moving the initial time t_1 along $\mathcal{M}_c$ from point 1 to point 3, the singularities Sg_n^+ simultaneously shift down avoiding the integration path because of their own divergence behaviour (see figure 3(*b*)). As a result, the end of the trajectory traverses the phase space from the transmissive quadrant ($P_2 < 0$, $Q_2 < 0$) to the reflective one ($P_2 > 0$, $Q_2 > 0$), as t_1 passes close to t_{1c} along $\mathcal{M}_c$. In other words, although the integration path C_1 is fixed, its topological nature with respect to the singularities changes during that process, thereby inducing the drastic change in the destination of the trajectory. (It should be remarked that, in the rigorous sense, the end point of the integration path moves with t_1, namely $s = t_2 - t_1 (t_2$ fixed), but its movement is negligible, because the distance between points 1 and 3 is negligibly small.) The set of end points of the trajectories with their initial points on $\mathcal{M}_c$, namely the corresponding $\mathcal{L}$-set, forms a *merged* object composed of the tunnelling and reflective branches, which should be defined along the topologically different paths C_1 and C_2 in the unperturbed limit, respectively [20–22].

4.3. Semiclassical results in the strong perturbation regime

In order to understand the relation between the critical point and fringed tunnelling in terms of the semiclassical theory, we have to see the global picture of the $\mathcal{M}$-set and $\mathcal{L}$-set. Figure 4(*a*) shows a typical example of the $\mathcal{M}$-set obtained in the strong perturbation regime, and figure 4(*b*) depicts the corresponding $\mathcal{L}$-set. On the t_1-plane (figure 4(*a*)), we can find three critical points each indicated by an X, which appear periodically with the period T ($= 2\pi/\omega$). Let us call them the first, second and third critical points in order from right to left. The structure of branches in the $\mathcal{M}$-set is very complicated, but we can easily recognize that the branch **1** passes very close to the first critical point. The first critical point and the branch **1** correspond to t_{1c} and $\mathcal{M}_c$ shown in figure 3(*a*), respectively. The branches **2** and **5** also run

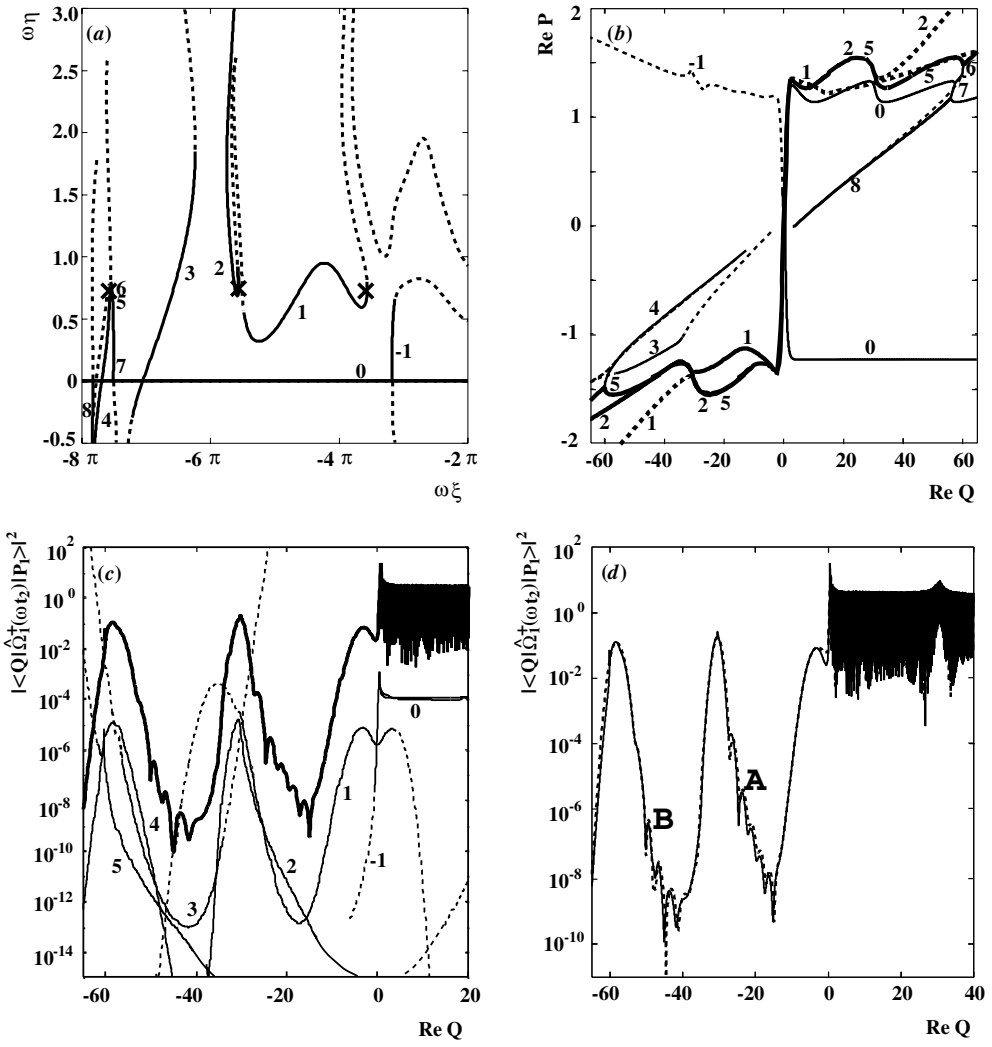

Figure 4. Results of the semiclassical calculation in the strong perturbation regime. The parameters are the same as in figure 3. (*a*) $\mathcal{M}$-set. The critical points are indicated by $\times$. (*b*) $\mathcal{L}$-set projected on to the real plane. The characteristic branches 1, 2 and 5 are drawn by thick lines. (*c*) The semiclassical probability amplitude (thick line) and weights of the branches (thin lines). The branches **1**, **2** and **3**, **4**, **5** interfere to yield the fringes of the tunnelling component (Re $Q < 0$). (*d*) The semiclassical probability amplitude (thick line) compared with the fully quantum probability amplitude (dashed line).

very close to the second and third critical points, respectively. The branch **5** is too small in this scale to identify, but its existence is confirmed in a magnified picture, which is not however shown here. Indeed, it is connected with branches **4** and **6** via caustics forming a chain structure, which is often observed as a typical structure of the complex branches contributing to the complex semiclassical formula [16, 17].

In the $\mathcal{L}$-set, all these branches, **1**, **2** and **5**, stretch over the reflective quadrant ($P > 0$, $Q > 0$) and the transmissive quadrant ($P < 0$, $Q < 0$), passing close to the origin. Then, as discussed above, they can be interpreted as the *merged* object composed of the tunnelling and

reflective branches of the unperturbed system. It should be noted that the parts of branches drawn by dashed lines indicate non-contributing parts which make unphysical contributions, and they can be removed by the proper treatment of the Stokes phenomenon (for details, see [19, 20]).

After such a procedure, we sum up all the contributions from the physically legal parts of the branches in the $\mathcal{M}$-set. The probabilistic weights of the branches together with the total probability obtained by the sum formula are shown in figure 4(c). All the probabilistic weights are multiplied by 10^{-4} for convenience of comparison with the total probability. In figure 4(d) the tunnelling probability obtained by the sum formula is compared with the result of the purely quantum computation. The semiclassical result reproduces every detail of the tunnelling wave including the complicated fringed patterns in the ranges indicated by A and B.

The appearance of fringes on the tunnelling component is the result of a simultaneous contribution of multiple tunnelling trajectories to the sum formula. Indeed, in the $\mathcal{L}$-set, we can find that two or more branches exist in the ranges of the fringed tunnelling, e.g. **1, 2** for A and **3, 4, 5** for B, and these groups of branches have nearly equal weights in the regions A and B, respectively (see figure 4(c)). The additional branches **3** and **4** contributing to the fringe are considered as those bifurcated from branch **2** in time evolution, and form a chain structure with **2** and **5**.

Therefore, the series of branches **1**, **2**, **5** respectively associated with the first, second and third critical points seems to play an important role in construction of interference fringes on the tunnelling component. In the $\mathcal{L}$-set, they traverse the phase space and thus contribute simultaneously to the wave-matrix. The simultaneous contribution results in the remarkable fringe pattern on the tunnelling wavefunction, if their weights are comparable.

5. Analyses of the critical point and the $\mathcal{M}$-set around it in the strong perturbation regime

In this section, we analytically clarify the underlying mechanism of the path-topology switching of the tunnelling trajectory and we answer the following question: why do the branches dominantly contributing to the fringed tunnelling appear by virtue of the strong perturbation? The critical point $t_1 = t_{1c}$ plays a key role in implementing the analyses. The detailed study of this object leads us to understanding characteristics of the critical point and the $\mathcal{M}$-set close to it, which are summarized as follows.

(1) The intersection between the CSM and the incident beam set $\mathcal{I} \equiv \{Q, P, t_1 | Q = Q_1, P = P_1, t_1 \in \mathbf{C}\}$ exists at an arbitrary perturbation strength, and if $t = t_{1c}$ is the intersection, then $t_{1c} + T$ (where T is the period of the perturbation) is also the intersection because of the periodic nature of the perturbation.

(2*a*) The intersection t_{1c} is the critical point of the singularities Sg_n^+ in the sense that the singularity diverges logarithmically as $Sg_n^+ \sim -\log(t_1 - t_{1c})/\nu$ at $t_1 = t_{1c}$.

(2*b*) In the close vicinity of any critical point there always exists a subset of the $\mathcal{M}$-set. We denote such a subset by $\mathcal{M}_c$.

(3) As t_1 is moved along $\mathcal{M}_c$, the end point of the trajectory $(Q(t_2 - t_1, t_1), P(t_2 - t_1, t_1))$ at $t = t_2$ traverses continuously but abruptly from the transmissive side to the reflective side (and vice versa) passing close to the origin O.

In the following, to clarify the above natures, theoretical analyses are developed by introducing the Melnikov method and an adiabatic solution in the low-frequency limit.

As will be discussed in the last part of the present section, the assertions of the above items lead us to understanding the underlying classical mechanism of the fringed tunnelling.

5.1. Item 1: intersection of CSM with the incident beam set

First, we would like to prove, by using the Melnikov method, that an intersection between the incident beam set and the stable manifold always exists in the complex domain, even if the strength of the perturbation is so small that an entanglement among them does not occur in the real phase space.

Let us divide the Hamiltonian into the unperturbed part and the perturbed part

$$H(Q, P, \omega t) = H_0(Q, P) + H_1(Q, t) \tag{5.1}$$

where

$$H_0 = P^2/2 + V_0(Q) \qquad H_1 = \epsilon v(Q, \omega t). \tag{5.2}$$

Both the unperturbed and perturbed systems have an unstable fixed point at the origin O because of the symmetry. (It should be noted that the unstable fixed point becomes an unstable periodic orbit if $\epsilon \neq 0$.) Let $(Q_s(t), P_s(t))$ be a trajectory on the stable manifold of the unstable point O, then $(Q_s(t), P_s(t))$ approaches O in the limit of $t \to \infty$.

Then the energy of the trajectory measured from O, which is denoted by ΔH_M, should be expressed by

$$\begin{aligned}\Delta H_M &\equiv H(Q_s(t), P_s(t), t) - H(Q = 0, P = 0, t) \\ &= \int_{\infty}^{t} \left\{ \frac{\partial H_1}{\partial t'}(Q_s(t'), t') - \frac{\partial H_1}{\partial t'}(Q = 0, t') \right\} \mathrm{d}t'.\end{aligned} \tag{5.3}$$

As the lowest-order approximation, the trajectory (Q_s, P_s) may be replaced by a trajectory on the unperturbed stable manifold (Q_{s0}, P_{s0}) given by equation (3.11), and ΔH_M is approximated by

$$\Delta H_M \sim \int_{\infty}^{t} \left\{ \frac{\partial H_1}{\partial t'}(Q_{s0}(t'), t') - \frac{\partial H_1}{\partial t'}(Q = 0, t') \right\} \mathrm{d}t' \tag{5.4}$$

which is nothing more than the Melnikov function [35] for scattering systems.

The energy at the origin is just the height of the time-dependent potential barrier:

$$a(t) \equiv H(Q = 0, P = 0, t) = 1 + \epsilon \sin(\omega t). \tag{5.5}$$

Using this together with equation (3.11), the Melnikov function (5.4) is evaluated, in the limit of $t - \mu \to -\infty$, as follows:

$$\Delta H_M(t) \sim -2\omega\epsilon \sin\omega\mu \int_0^{\infty} \frac{\sin \omega s}{1 + \mathrm{e}^{2\sqrt{2}s}} \mathrm{d}s - a(t) + a(\mu). \tag{5.6}$$

Finally from equations (5.3), (5.5) and (5.6), the energy at the initial time $t = t_1$ is given by

$$H(t_1) \sim 1 + \epsilon(1 - \chi(\omega)) \sin\omega\mu \tag{5.7}$$

where

$$\chi(\omega) \equiv 2\omega \int_0^{\infty} \frac{\sin \omega s}{1 + \mathrm{e}^{2\sqrt{2}s}} \mathrm{d}s \tag{5.8}$$

and μ and t_1 are related by equation (3.12).

Let us see a numerical result. Figure 5 depicts the CSM calculated by using equation (5.7), which forms a 2D surface in the 3D space, where the axes x, y and z indicate $\mathrm{Re}\, E_1$, $\mathrm{Re}\, \mu$ and $\mathrm{Im}\, \mu$, respectively. Note that for visualization the axis of $\mathrm{Im}\, E_1$ is omitted in the picture.

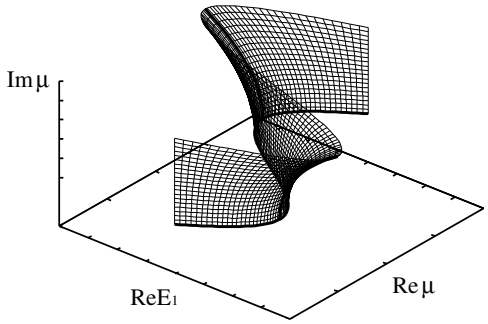

Figure 5. Complexified stable manifold calculated by the Melnikov method.

The curved bottom line ($\mathrm{Im}\,\mu = 0$) indicates the real stable manifold. The energy on the CSM is no longer real valued, thus it takes a real value only on 1D curves drawn by thick lines, which form ridge and valley lines of the surface. Since the initial energy $E_1\left(=P_1^2/2\right)$ takes a real value on the incident beam set, then μ_c at which $H(t_1(\mu_c) = t_{1c}) = E_1 \in \mathbf{R}$ should be located at a point on the ridge or valley line or the bottom line. Indeed, the crossing condition for μ_c between the stable manifold and the incident beam set is given as follows:

$$E_1 = P_1^2/2 = 1 + \epsilon(1 - \chi(\omega))\,\sin\omega\mu_c. \tag{5.9}$$

Using the definition of the parameter μ given by equation (3.12), the intersection t_{1c} is decided as the lowest-order approximation by the above relation. When E_1 is considerably less than 1, the real intersections, i.e. $\mathrm{Im}\,t_{1c} = \mathrm{Im}\,\mu_c = 0$, exist only for a sufficiently strong perturbation strength such that $\epsilon \geqslant \epsilon_{th} \equiv |(1 - E_1)/(1 - \chi(\omega))|$, but if the intersection is allowed to be complex, it may exist at an arbitrarily weak perturbation strength. Indeed, the complexified intersections μ_c are decided as

$$\omega\,\mathrm{Re}\,\mu_c = 3\pi/2 + 2n\pi \tag{5.10}$$

$$\cosh(\omega\,\mathrm{Im}\,\mu_c) = \epsilon^{-1}(1 - E_1)/(1 - \chi(\omega)). \tag{5.11}$$

In other words, the complex intersections

$$\mathrm{Re}\,t_{1c} = \mathrm{Re}\,\mu_c - (Q_1 - \log 2)/\sqrt{2} = (3/2 + 2n)\pi/\omega - (Q_1 - \log 2)/\sqrt{2} \tag{5.12}$$

$$\mathrm{Im}\,t_{1c} = \mathrm{Im}\,\mu_c = \omega^{-1}\cosh^{-1}\{\epsilon^{-1}(1 - E_1)/(1 - \chi(\omega))\} \tag{5.13}$$

exist periodically at the interval $T = 2\pi/\omega$, even if the real intersections disappear in the weaker range of perturbation such that $\epsilon < \epsilon_{th}$. We comment that the evaluation of equation (5.13) agrees well with the numerical estimation of $\mathrm{Im}\,t_{1c}$.

5.2. Item 2: a solution of the low-frequency-limit

5.2.1. Low-frequency approximation. In this section we justify the two assertions summarized by items (2*a*) and (2*b*). For this purpose we introduce an approximate fully-nonlinear solution which is correct in the low-frequency limit of the perturbation ($\omega \ll 1$). Using the solution, we prove the two assertions. Our treatment is approximate but provides a consistent scenario which describes what happens close to the critical point.

It should be noted that in a previous paper [21] we have given a brief sketch of the proofs of items (2*a*) and (2*b*) based upon the linear approximation in the neighbourhood of the unstable

fixed point. The linear theory is quite general and is independent of details of a model system, but it contains some basic assumption about the relation between the scattering region and the asymptotic region. The fully-nonlinear approach presented here overcomes such an essential defect.

Now, we assume the following form of the solution which can be considered as a natural extension of the unperturbed solution equation (3.1):

$$\sinh Q(t) = r(t)\cosh\phi(t). \tag{5.14}$$

We substitute it into the equation of motion

$$\ddot{Q} = 2a(t)\frac{\sinh Q}{\cosh^3 Q} \tag{5.15}$$

where $a(t)$ is defined by equation (5.5), and the equation

$$\frac{\mathrm{d}}{\mathrm{d}t}\{r^2\dot{\phi}\}\sinh(\phi) - [2E(t) - \dot{\phi}^2]r^2\cosh(\phi) + r\ddot{r}\cosh(\phi) = 0 \tag{5.16}$$

immediately follows. The low-frequency approximation (or adiabatic approximation) means negligibility of the third term containing the second-order derivative of the *amplitude* r. We first decide the *phase variable* ϕ by the relation

$$\dot{\phi}(t) = \sqrt{2E(t)} \tag{5.17}$$

then equation (5.16) is reduced to

$$\frac{\mathrm{d}}{\mathrm{d}t}\{r(t)^2\dot{\phi}(t)\} = 0 \qquad \text{namely} \qquad r(t) = \frac{\alpha}{\{2E(t)\}^{1/4}} \tag{5.18}$$

where α is a certain constant of motion, which is decided by the initial condition. Equation (5.18) implies that the adiabatic approximation dropping $\frac{\mathrm{d}^2 r(t)}{\mathrm{d}t^2}$ is equivalent to neglecting the second-order derivative $\frac{\mathrm{d}^2 E(t)}{\mathrm{d}t^2}\big/E(t)$ compared with $\frac{\mathrm{d}E(t)}{\mathrm{d}t}\big/E(t)$. Equation (5.17) is solved simultaneously with the energy gain equation, i.e.

$$\frac{\mathrm{d}E(t)}{\mathrm{d}t} = \dot{a}(t)h(t) \tag{5.19}$$

where

$$h(t) = \{\cosh^2 Q(t)\}^{-1} = \{1 + r(t)^2\cosh^2\phi(t)\}^{-1} \tag{5.20}$$

under the initial condition ($\phi_0 = \phi(t_0)$, $E_0 = E(t_0)$) at $t = t_0$, which is conventionally taken in the scattering region. We have three free parameters, ϕ_0, E_0 and α, but E_0 and α are not independent of each other. To show this we see that the momentum $P(t) = \frac{\mathrm{d}Q(t)}{\mathrm{d}t}$ is given by

$$P(t) = \sqrt{2E}r(t)\sinh(\phi(t))/\cosh Q(t) \tag{5.21}$$

neglecting the correction of $O(\epsilon\omega)$, and substitution of equations (5.14) and (5.21) into the expression of the energy $E = P^2/2 + a(t)/\cosh^2 Q$ yields the relation

$$E_0 = a(t_0)/\{1 + \alpha^2/\sqrt{2E_0}\}. \tag{5.22}$$

Without loss of generality, we may choose t_0 as the time at which the phase vanishes $\phi(t_0) = 0$. In the unperturbed limit, t_0 is the time when the trajectory reaches the turning point.

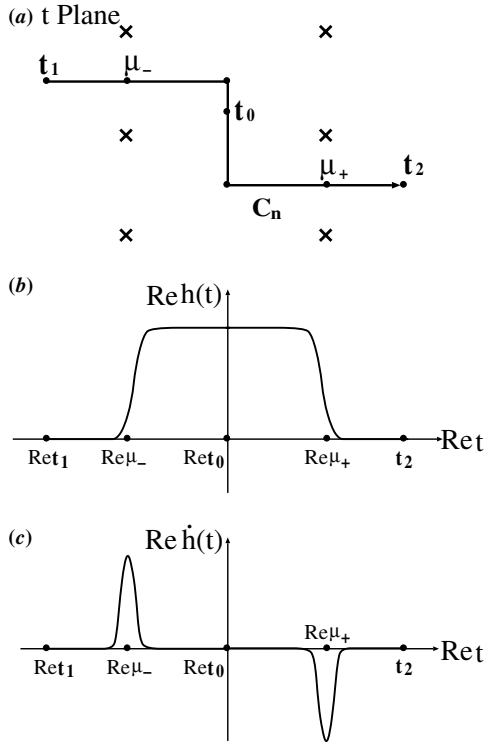

Figure 6. Behaviour of the function $h(t)$ defined by equation (5.20) near the gate $\mu_{\mp}$. (*a*) Positions of the gates $\mu_{\mp}$ on the complex t plane. An integration path C_n passing through the gates $\mu\mp$ is also drawn. (*b*) $\mathrm{Re}\,h(t)$ along the path C_n. Note that, if $|\alpha| \ll 1$, then $|\mathrm{Re}\,h(t)| \gg |\mathrm{Im}\,h(t)|$. (*c*) $\mathrm{Re}\,\dot{h}(t)$ along the path C_n.

5.2.2. Gates of the scattering region, and estimation of energy and phase variables. If we neglect the perturbation, then $E(t) = E_0 = \text{const}$, and $\phi(t)$ and $r(t)$ are expressed as

$$\phi(t) = \sqrt{2E_0}(t - t_0) \qquad \text{and} \qquad r(t) = \alpha/(2E_0)^{1/4} \tag{5.23}$$

from equations (5.17) and (5.18). With these approximations, we examine the feature of the function $h(t)$, which plays a key role in the dynamics dictated by equations (5.17) and (5.18) through equation (5.19). The integration path is taken so as to go between the singularities. Generally including the case of $\epsilon \neq 0$ as well, it is convenient to make it pass through the two points $\mu_{\mp}$ called 'gates', which are defined by

$$\mathrm{d}^2h(t)/\mathrm{d}\phi^2|_{t=\mu_{\mp}} = 0 \tag{5.24}$$

where the differentiation is executed regarding t as the function of ϕ (see appendix A for more details). In the case of $\epsilon = 0$, equation (5.24) is equivalent to $\mathrm{d}^2h(t = \mu_{\mp})/\mathrm{d}t^2 = 0$ (see equation (5.23)), and $\mu_{\mp}$ are just the middle points of two adjacent singularities $t_{sg}\left(= Sg_n^{\mp} + t_1\right)$ and $t'_{sg}\left(= Sg_{n+1}^{\mp} + t_1\right)$, which are the times making $h(t)$ (or potential) singular, namely, $\cosh\phi(t_{sg}) = \pm\mathrm{i}/r$ (see section 3.2). Substitution of equation (5.20) into equation (5.24) together with equation (5.22) implies that $\mu_{\mp}$ are decided as functions of α and t_0. If the integration path is parallel to the real axis in neighbourhoods of $\mu_{\mp}$ (see figure 6(*a*)), $h(t)$ increases abruptly from 0 to a constant close to 1 at μ_- and decreases from the constant to zero at μ_+ (see figure 6(*b*)). From equation (5.19) with equation (5.20), the energy gain (or loss)

along the integration path occurs only in the scattering region between the two gates; then, the gates μ_- and μ_+ are called the entrance and exit gates, respectively. Note that μ_- becomes the parameter μ defined for the unperturbed system by equation (3.12) in the limit $\alpha \to 0$ and $\epsilon \to 0$. The particle travels freely at a constant momentum outside the gates, whereas it is perturbed by the scattering potential inside the gates. Such a definite feature makes it easier to evaluate both $\phi(t)$ and $E(t)$ in the practical calculation. Indeed, as is fully described in appendix A in detail, the time-dependent energy is expressed as

$$E(t) = \begin{cases} a(t)h(t) - a(\max_R\{t, \mu_-\})(h(t) - h(t_0)) & (\text{if } \mathrm{Re}\{t - t_0\} < 0) \\ a(t)h(t) - a(\min_R\{t, \mu_+\})(h(t) - h(t_0)) & (\text{if } \mathrm{Re}\{t - t_0\} > 0) \end{cases} \tag{5.25}$$

where a small correction of $O(\epsilon\omega)$ is neglected in the adiabatic limit. $\max_R$ and $\min_R$ are respectively defined by

$$\begin{aligned} \max_R(z_1, z_2) &= \begin{cases} z_1 & \text{if} \quad \mathrm{Re}\{z_1 - z_2\} \geqslant 0 \\ z_2 & \text{if} \quad \mathrm{Re}\{z_2 - z_1\} < 0 \end{cases} \\ \min_R(z_1, z_2) &= \begin{cases} z_2 & \text{if} \quad \mathrm{Re}\{z_1 - z_2\} \geqslant 0 \\ z_1 & \text{if} \quad \mathrm{Re}\{z_2 - z_1\} < 0 \end{cases} . \end{aligned} \tag{5.26}$$

Using equation (5.25) in equation (5.17) and integrating it, $\phi(t)$ is expressed in the following form

$$\phi(t) = \int_{t_0}^{\mu_-} \mathrm{d}s \sqrt{2a(s)h(t_0)} + \sqrt{2a(\mu_-)h(t_0)}(t - \mu_-) \qquad (\text{if } \mathrm{Re}\{t\} \leqslant \mathrm{Re}\{\mu_-\}) \tag{5.27}$$

$$\phi(t) = \int_{t_0}^{t} \mathrm{d}s \sqrt{2a(s)h(t_0)} \qquad (\text{if } \mathrm{Re}\{\mu_-\} \leqslant \mathrm{Re}\{t\} \leqslant \mathrm{Re}\{\mu_+\}) \tag{5.28}$$

$$\phi(t) = \int_{t_0}^{\mu_+} \mathrm{d}s \sqrt{2a(s)h(t_0)} + \sqrt{2a(\mu_+)h(t_0)}(t - \mu_+) \qquad (\text{if } \mathrm{Re}\{t\} \geqslant \mathrm{Re}\{\mu_+\}) \tag{5.29}$$

where terms of $O(\epsilon\omega)$ are omitted again.

Here we note that, by taking the limit $\alpha \to 0$, the solution describes the family of trajectories on the stable manifold of the unstable fixed point O. For this purpose, we consider the local behaviour of the solution close to O by taking t inside the two gates, then the linear approximation, i.e. $\sinh Q \sim Q$ and $\mathrm{sech} Q \sim 1$, can be applied. Indeed, equations (5.14) and (5.21) together with equations (5.18), (5.25) and (5.28) yield

$$\begin{aligned} Q(t) &= \alpha^2 \chi_+(t)\, \mathrm{e}^{\nu(t-\bar{\mu}_-)} + \chi_-(t)\, \mathrm{e}^{-\nu(t-\bar{\mu}_-)} \\ P(t) &= \sqrt{2a(t)}[\alpha^2 \chi_+(t)\, \mathrm{e}^{\nu(t-\bar{\mu}_-)} - \chi_-(t)\, \mathrm{e}^{-\nu(t-\bar{\mu}_-)}] \end{aligned} \tag{5.30}$$

where the estimation

$$h(t_0) = 1 - \alpha^2/\sqrt{2} + O(\alpha^2\epsilon) + O(\alpha^4) \to 1 \ (\alpha \to 1) \tag{5.31}$$

obtained by equation (5.20) with equations (5.18), (5.25) and (5.22) is used, and

$$\begin{aligned} &\nu \equiv \frac{1}{T}\int_0^T \sqrt{2a(s)}\, \mathrm{d}s \qquad \sigma(t) \equiv \int_0^t [\sqrt{2a(s)} - \nu]\, \mathrm{d}s \\ &\bar{\mu}_- \equiv [\log\alpha + \sigma(t_0)]/\nu + t_0 \end{aligned} \tag{5.32}$$

where $\sigma(t) = \sigma(t + T)$ is a periodic function of $O(\epsilon/\omega)$, and

$$\chi_\pm(t) \equiv \exp(\pm\sigma(t))/\{2[2a(t)]^{1/4}\}. \tag{5.33}$$

We fix the parameter $\bar{\mu}_-$ and take the limit $\alpha \to 0$, then equation (5.30) represents a stable trajectory exponentially approaching O. The complex 1D (real 2D) manifold made up from such trajectories by scanning the free parameter $\bar{\mu}$ in $\mathbf{C}$ forms the local stable manifold in the close vicinity of O. The set of equations (5.14) and (5.21), which are the global extension of the local solution, thus represents a globally extended stable manifold in the limit of $\alpha \to 0$.

5.2.3. Parameters controlling the distance from the critical point. Now in order to decide the relation among the parameters μ_-, t_1 and α, we take into account the boundary condition, $P = P_1$, $Q = Q_1$ at $t = t_1$. From equation (5.25) the relation

$$E_1 = P_1^2/2 = a(\mu_-)h(t_0)(=E(\mu_-)) \sim a(\mu_-)[1 - \alpha^2/\sqrt{2}] \tag{5.34}$$

follows, where the estimation $h(t_0) \sim 1 - \alpha^2/\sqrt{2}$ given by equation (5.31) is used. Then, μ_- is approximately obtained as a function of α and E_1. From the definition of $\mu_\pm$ (equation (5.24)), $\phi_\pm = \phi(\mu_\pm)$ are reduced to (see equation (A.1) in appendix A)

$$\mathrm{e}^{\pm\phi(\mu_\pm)} = 2\,\mathrm{e}^{\mathrm{i}n_\pm\pi}[1 + r(\mu_\pm)^2/4 + O(|\alpha|^4)]/r(\mu_\pm) \tag{5.35}$$

where $n_\pm$ are integers decided by the choice of the integration path, i.e. the imaginary depths of the gates μ_+ and μ_-. By using the boundary condition $Q(t_1) = Q_1(\gg 1)$, i.e.,

$$\sinh(Q_1) = r(t_1)\cosh\phi(t_1) \to \mathrm{e}^{Q_1} = r(t_1)\,\mathrm{e}^{-\phi(t_1)} = \alpha(2E_1)^{-1/4}\,\mathrm{e}^{-\phi(t_1)} \tag{5.36}$$

and the relation $\phi(t_1) - \phi(\mu_-) = (t_1 - \mu_-)\sqrt{2h(t_0)a(\mu_-)}$ (equation (5.27)), together with equations (5.34) and (5.35) at $n_- = 0$, we can obtain the relation between t_1 and μ_-,

$$\sqrt{2E_1}(t_1 - \mu_-) + Q_1 = \log 2 + \alpha^2\{4\sqrt{2E_1}\}^{-1}. \tag{5.37}$$

Equations (5.34) and (5.37) provide a set of equations deciding t_1 and μ_- as functions of α. Remember that the solution is on the stable manifold in the limit $\alpha \to 0$. Therefore, the intersection t_{1c} of the stable manifold with the incident beam set is obtained by setting $\alpha = 0$ in both equations. Indeed, with $\alpha = 0$ equation (5.34) coincides with equation (5.9) derived by the Melnikov method, if the term of $O(\epsilon\omega)$ in equation (5.9) is dropped according to the spirit of adiabatic approximation.

Let t_{1c} and μ_{-c} be t_1 and μ_- at $\alpha = 0$, respectively, then from equations (5.34) and (5.37) we obtain a key result relating the smallness parameter α^2 to the deviation of t_1 from t_{1c}

$$\alpha^2 = A_1(t_1 - t_{1c}) = A_2(\mu_- - \mu_{-c}) \tag{5.38}$$

where

$$A_1 \sim A_2 = \sqrt{2}\{a(\mu_{-c})\}^{-1}\left.\frac{\mathrm{d}a(\mu_-)}{\mathrm{d}\mu_-}\right|_{\mu_-=\mu_{-c}} \tag{5.39}$$

is a constant of $O(\epsilon\omega)$, which is controlled by the amplitude of the periodic perturbation. Now the significance of the smallness parameter α^2 is clarified in terms of the boundary condition, and terms of $O(|\alpha|^2)$ giving no quantitatively significant effect on the calculation of the phase factor $\phi(t)$ will be neglected, namely the approximation $h(t_0) = 1$ is used in the following. For convenience of the following arguments, we introduce

$$\varphi(t) = \phi(t) + \log 2 - \log\{\alpha(2E(t))^{-1/4}\}. \tag{5.40}$$

Then according to the similar manipulations shown above, we can derive explicit expressions of $\phi(t)$ or $\varphi(t)$ by using the boundary condition equations (5.34) and (5.36) for equation (5.27)

and further combining it with equations (5.28) and (5.29)

$$\varphi(t) = \begin{cases} \sqrt{2E_1}(t-t_1) - Q_1 + \log 2 & (\text{if } \mathrm{Re}\, t \leqslant \mathrm{Re}\, \mu_-) \\ \nu(t-\mu_-) + \sigma(t) - \sigma(\mu_-) + \frac{1}{4}\log\frac{a(t)}{E_1} + \varphi(\mu_-) & (\text{if } \mathrm{Re}\, \mu_- \leqslant \mathrm{Re}\, t \leqslant \mathrm{Re}\, \mu_+) \\ \sqrt{2a(\mu_+)}(t-\mu_+) + \varphi(\mu_+) & (\text{if } \mathrm{Re}\, t \geqslant \mathrm{Re}\, \mu_+) \end{cases} \tag{5.41}$$

where the exponent ν and the periodic component $\sigma(t)$ are defined by equation (5.32), and we make use of the relation

$$E(t) = \begin{cases} a(\mu_-) = E_1 & (\text{if } \mathrm{Re}\, t \ll \mathrm{Re}\, \mu_-) \\ a(t) & (\text{if } \mathrm{Re}\, \mu_- \leqslant \mathrm{Re}\, t \leqslant \mathrm{Re}\, \mu_+) \\ a(\mu_+) & (\text{if } \mathrm{Re}\, t \gg \mathrm{Re}\, \mu_+) \end{cases} \tag{5.42}$$

which immediately follows from equation (5.25). It is easily shown from equations (5.37) and (5.41) that the newly introduced phase $\varphi(t)$ almost vanishes at $t = \mu_-$:

$$\varphi(\mu_-) = -\alpha^2\{4\sqrt{2E_1}\}^{-1} \sim 0. \tag{5.43}$$

With the use of $\varphi(t)$, the trajectory expressed by equations (5.14) and (5.21) is rewritten in the following form

$$\sinh Q(t) = \alpha^2\, \mathrm{e}^{\varphi(t)}/(4\sqrt{2E(t)}) + \mathrm{e}^{-\varphi(t)} \tag{5.44}$$

$$P(t) = \operatorname{sech} Q(t)[\alpha^2\, \mathrm{e}^{\varphi(t)}/4 - \sqrt{2E(t)}\, \mathrm{e}^{-\varphi(t)}] \tag{5.45}$$

where equations (5.18) and (5.40) are used. Suppose $|Q(t)| \ll 1$, then $\sinh Q$ and $\operatorname{sech} Q$ may be replaced by Q and 1, respectively. Such a condition is fulfilled, when $\mathrm{Re}\, \mu_- \ll \mathrm{Re}\, t \ll \mathrm{Re}\, \mu_+$. With this approximation, substitution of the second formula of equation (5.41) with equation (5.43) into the above equations results in the linearized solution (5.30), where the parameter μ_-, which approaches to the fixed value μ_{-c} in the limit of $\alpha \to 0$, is identified with $\bar{\mu}_-$ (rigorously, shifted by an amount).

5.2.4. Item 2a: gates, singularities and logarithmic divergence. Suppose $\mathrm{Re}\, \mu_- \leqslant t \leqslant \mathrm{Re}\, \mu_+$, then $E(t)$ and $\phi(t)$ are expressed by equations (5.25) and (5.28), respectively, and equation (5.35) gives the relative location of gates with respect to t_0

$$\pm(\mu_\pm - t_0) = \nu^{-1}\{\mathrm{i}n_\pm\pi - \log\{\alpha/(2^{5/4})\} \mp \sigma(\mu_\pm) \pm \sigma(t_0) + \log a(\mu_\pm)^{1/4}\} \tag{5.46}$$

where ν and $\sigma(t)$ are defined by equation (5.32). The entrance and exit gates are respectively aligned on different lines parallel to the imaginary axis, on which they are arranged approximately at the interval $\sim \mathrm{i}\pi/\nu$. Thus, the difference of two sorts of gates is

$$\mu_+ - \mu_- = -\frac{\log(\alpha^2/2^{5/2}) - \mathrm{i}(n_+ + n_-)\pi}{\nu} + \Delta\mu\left(-\frac{\log(\mathrm{e}^{-\mathrm{i}(n_+ + n_-)\pi}\alpha^2/2^{5/2})}{\nu}, \mu_-\right) \tag{5.47}$$

where the small correction $\Delta\mu(x, y)$ of $O(\epsilon)$ is a periodic function of both x and y with the period T approximately given by $\Delta\mu(x, y) = [-\sigma(x+y) + \sigma(y) + \log\{a(x+y)a(y)\}/4]/\nu$.

Next, we consider the singularities $t_{sg}\left(=Sg_n^\pm + t_1\right)$ of the trajectory, namely, the time at which it hits the coordinate $Q = Q_{sg}$ making the potential diverge. In the limit of $\epsilon = 0$, they are separated from the gates $\mu_\pm$ by $\pm\mathrm{i}\pi/(2\sqrt{2E_1})$. Application of the oscillatory perturbation does not change such a character. Indeed, as shown in appendix B, the singularities are sited within a finite bounded distance from μ_+ or μ_-, which is insensitive to α

$$|\Delta t_{sg}| < M/\sqrt{E_1} \qquad \text{where} \qquad \Delta t_{sg} \equiv t_{sg} - \mu_+ \,(\text{or } \mu_-) \tag{5.48}$$

and M is a finite constant of $O(1)$. On the other hand, the distance of μ_+ from μ_- diverges logarithmically as α goes to zero, which means that the singularities $Sg_n^+ = t_{sg} - t_1$ neighbouring the exit gate μ_+ also diverge following μ_+:

$$Sg_n^+ = -\{\log(\alpha^2/2^{5/2}) - \mathrm{i}n\pi\}/\nu + \mu_{-c} - t_{1c} + \Delta t_{sg} + \Delta\mu(-\log(\mathrm{e}^{-\mathrm{i}\pi n}\alpha^2/2^{5/2})/\nu, \mu_-) \quad (n : \text{integer}). \tag{5.49}$$

Here, equations (5.47) and (5.48) are used, and t_1 and μ_- are replaced by t_{1c} and μ_{-c}, respectively, because we suppose $t_1 \sim t_{1c}$, i.e. $|\alpha^2| \to 0$. Hence, item (2a) is proven. We remark that the negative singularities Sg_n^- neighbouring the entrance gate μ_- do not of course diverge.

5.2.5. Item 2b: the subset $\mathcal{M}_c$. We show that a subset of $\mathcal{M}$, which is denoted by $\mathcal{M}_c$, in general passes close to the critical point. We suppose $\mathrm{Re}\, t \leqslant \mathrm{Re}\, \mu_+$, then the second equation of equation (5.41) is available, and from equation (5.43) we obtain

$$\varphi(t) = \nu(t - \mu_{-c}) + \sigma(t) - \sigma(\mu_{-c}) + \log\{a(t)/E_1\}^{1/4} \tag{5.50}$$

where the parameters such as μ_- and t_1 depending very weakly on $\alpha^2 = A_2(\mu_- - \mu_{-c}) = A_1(t_1 - t_{1c})$ (see equation (5.38)) are replaced by μ_{-c} and t_{1c}, respectively. Thus, $\varphi(t)$ (and $E(t)$, of course) depends only on t, and is *independent of* t_1. Significant dependence of the trajectory ((5.44) and (5.45)) on t_1 comes from the parameter α^2. More explicitly, the coordinate, for example, depends on t and t_1 as

$$\sinh Q(t - t_1, t_1) = A_1(t_1 - t_{1c})\,\mathrm{e}^{\varphi(t)}/(4\sqrt{2a(t)}) + \mathrm{e}^{-\varphi(t)}. \tag{5.51}$$

The $\mathcal{M}$-set is the set of t_1 satisfying the boundary condition, $\sinh Q(t_2 - t_1, t_1) = Q_2 \in \mathbf{R}$ at a fixed $t = t_2 \in \mathbf{R}$. Setting $Y \equiv \sinh Q_2$, where Y is an arbitrary real number, it immediately follows

$$t_1 - t_{1c} = \alpha^2/A_1 = (C_1 Y - C_2)/A_1 \tag{5.52}$$

with

$$C_1 = 4\sqrt{2E(t_2)}\,\mathrm{e}^{-\varphi(t_2)} \qquad C_2 = 4\sqrt{2E(t_2)}\,\mathrm{e}^{-2\varphi(t_2)} \tag{5.53}$$

and the set of t_1 satisfying equation (5.52) forms a straight line on the complex t_1 plane parametrized by $Y = \sinh Q_2 \in \mathbf{R}$.

Since ϵ is sufficiently less than 1, φ is well approximated by the first term of the right-hand side of equation (5.50), i.e. $\varphi_2 \equiv \varphi(t_2) \sim \nu(t_2 - \mu_{-c})$. Thus, by taking $t_2 \gg \mathrm{Re}\, \mu_{-c}$, we can make $\mathrm{Re}\, \varphi_2$ large enough, so that the straight line sits at a very small distance $|C_2/A_1| \sim \mathrm{e}^{-2\mathrm{Re}\,\varphi_2}/|A_1|$ from t_{1c}, which is the set $\mathcal{M}_c$ introduced in the assertion of item (2b).

A question arising here concerns the possibility of choosing t_2 such that $t_2 \leqslant \mathrm{Re}\, \mu_+$ and $t_2 - \mathrm{Re}\, \mu_- \gg 1$. In the next subsection we show that it is possible.

5.3. Item 3: characteristic neighbourhood of the critical point and switching of path topology

Taking into account all the results in the above analyses, we arrive at a satisfactory understanding of the remarkable features in the strong coupling regime, i.e. the divergent behaviour of the singularities and the merger of the transmissive and reflective branches.

Let us fix the observatory time $t_2 (\gg \mathrm{Re}\, \mu_-) \in \mathbf{R}$, and consider a half line beginning at t_{1c} and going away in any direction on the t_1-plane. Let t_1 approach t_{1c} along the line, then the parameter α^2 goes to zero (equation (5.38)), and the real part of μ_+ shifts divergently in the positive direction because $\mathrm{Re}\{\mu_+ - \mu_-\} \sim -\frac{1}{\nu}\log|A_1(t_1 - t_{1c})|$ (from equations (5.38) and (5.47)). For an arbitrary large t_2, there must be a point on the half line, beyond which $\mathrm{Re}\{\mu_+\}$

always exceeds t_2. Consequently, there exists a characteristic neighbourhood of the critical point on the t_1-plane, say $B(t_2)$; if t_1 is taken inside $B(t_2)$, then the end of the integration path is inside the region between the two gates, μ_- and μ_+, whereas it is out of the gate μ_+, if t_1 is outside $B(t_2)$. The boundary of $B(t_2)$ is thus defined by

$$t_2 = \mathrm{Re}\{\mu_+\} = \mathrm{Re}\{\mu_+ - \mu_-\} + \mathrm{Re}\{\mu_-\} \sim \mathrm{Re}\,\{-\nu^{-1}\log\alpha^2 + \mu_-\}. \tag{5.54}$$

Substitution of equation (5.38) gives the radius of the region $B(t_2)$,

$$|t_1 - t_{1c}| \sim \mathrm{e}^{-\nu(t_2 - \mathrm{Re}\,\mu_{-c})}/|A_1| \tag{5.55}$$

where μ_- is replaced by μ_{-c}, because $t_1 \to t_{1c}$. As discussed in section 5.2.5, the distance of the subset $\mathcal{M}_c$ from t_{1c} is given by $|C_2/A_1| \sim \mathrm{e}^{-2\,\mathrm{Re}\,\varphi_2}/|A_1| \sim \mathrm{e}^{-2\nu(t_2 - \mathrm{Re}\,\mu_{-c})}/|A_1|$, which is much less than the radius. Since $\mathcal{M}_c$ exists forming a straight line inside $B(t_2)$ (see equation (5.52)), then it should intersect the boundary of $B(t_2)$ at two points.

From equation (5.48) the distance between μ_+ and the closest singularity is finitely bounded, $\mathrm{Re}\,\{\mu_+ - t_1\}$ may be identified with $\mathrm{Re}\{Sg_n^+\}$, and whether t_1 is in $B(t_2)$ or not corresponds respectively to

$$\mathrm{Re}\{s\} < \mathrm{Re}\left\{Sg_n^+\right\} \qquad \text{or} \qquad \mathrm{Re}\{s\} > \mathrm{Re}\left\{Sg_n^+\right\} \tag{5.56}$$

where $s = t_2 - t_1$ is the lapse time.

The outside of $B(t_2)$ corresponds to the asymptotic region, while the inside is mapped on to the scattering region. As shown in figure 7(a), we take two points on $\mathcal{M}_c$, say **a'** and **c'**, in opposite sides out of $B(t_2)$, and let t_1 move along $\mathcal{M}_c$ from **a'** to **c'** going through the region inside $B(t_2)$. We put further some marks on $\mathcal{M}_c$: two intersections **a, c** and the point **b** closest to t_{1c}.

Now we can reproduce the numerically observed behaviour of the singularities around the integration path C_n as shown in figure 7(b). As t_1 moves along $\mathcal{M}_c$ going across **b**, α^2 varies according to equation (5.52), i.e. $\alpha^2 = A_1(t_1 - t_{1c}) = C_1 Y - C_2$. The key is that the end of the integration path $s = t_2 - t_1$ does not move very significantly, because the variable t_1 moves in quite a restricted range, whereas from equation (5.49) the singularity Sg_n^+ is very sensitive to t_1 as

$$Sg_n^+ \sim -\nu^{-1}\,\log A_1(t_1 - t_{1c}) = -\nu^{-1}\,\log(C_1 Y - C_2). \tag{5.57}$$

First, Sg_n^+ moves on the s-plane to the positive real side. Its real part overtakes $\mathrm{Re}\,s\,(=t_2 - t_1)$ at **a** (equation (5.54)), and further it increases divergently to reach the maximum as t_1 passes **b** at $Y \sim 0$. As t_1 approaches **c'**, the real part returns to the initial value at **a'**, but its imaginary part shifts by $\pm\mathrm{i}\pi/\nu$, i.e. the fundamental interval of the singularities Sg_n^+. Thus, all the singularities Sg_n^+, which are aligned on a line, make a detour avoiding the integration path and eventually shift by their fundamental interval in the imaginary direction. The topology of the integration path with respect to the singularities is switched abruptly but continuously by such a divergent detour of the singularities. As discussed in section 4.2, the occurrence of the drastic phenomenon means that the branches of the $\mathcal{M}$-set corresponding to the transmitted trajectories and the reflected trajectories, which are separated in the unperturbed limit, are merged to form a unified branch connecting the transmissive and reflective ones.

In the present formulation, the continuous switch from the transmitted trajectory to the reflected trajectory (and vice versa) along $\mathcal{M}_c$ can be understood immediately. The movement of t_1 along $\mathcal{M}_c$ from **a** to **c** means a change of the real parameter Y from a negative (positive) value of $O(1)$ to a positive (negative) value of $O(1)$, changing its sign. In such a process, the set of coordinate and momentum at the end of the trajectory, i.e.,

$$Q_2 = \sinh^{-1} Y \qquad P_2 = \sqrt{2a(t_2)}\{Y - 2\,\mathrm{e}^{-\varphi(t_2)}\}\mathrm{sech}\,Q_2 \sim \sqrt{2}Y\mathrm{sech}(\sinh^{-1} Y) \tag{5.58}$$

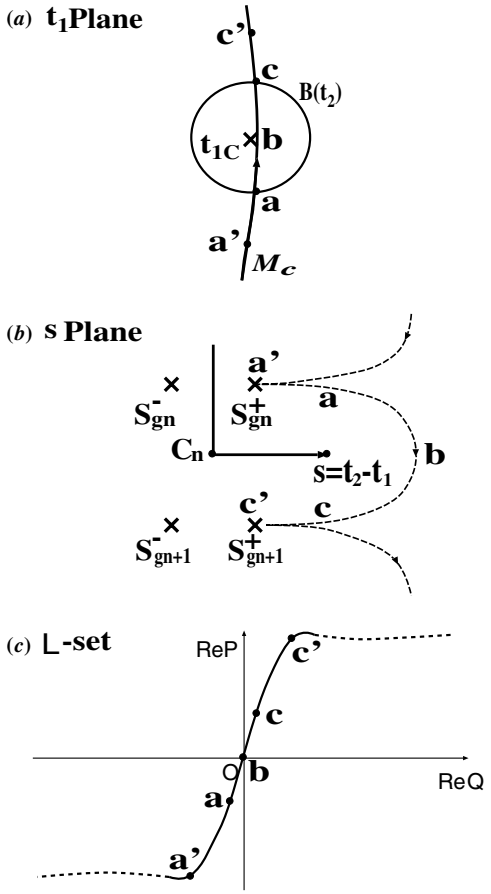

Figure 7. Switching of the path-topology. (*a*) Characteristic neighbourhood of the critical point $B(t_2)$ and the subset passing through it $\mathcal{M}_c$. (*b*) Movement of the singularities Sg_n^+. They diverge detouring around the integration path C_n as t_1 passing through $B(t_2)$ along $\mathcal{M}_c$. (*c*) Movement of the end point of the trajectory projected on the real phase space as t_1 moving along $\mathcal{M}_c$.

which is obtained by setting $t = t_2$ in equation (5.45) and using $a(t_2) = E(t_2)$, traverses the phase space from the transmissive quadrant (Re $Q_2 < 0$, Re $P_2 < 0$) to the reflective quadrant (Re $Q_2 > 0$, Re $P_2 > 0$), and vice versa (see figure 7(*c*)).

Now we come to a complete understanding of mechanism of the path-topology switching caused by the divergent detour of the singularities Sg_n^+, which was demonstrated numerically in section 4.2.

5.4. Global structure of branches and classical mechanism of the fringed tunnelling

In this subsection, based upon the analyses developed in the above subsections, we consider the classical mechanism of the fringed tunnelling. The numerical results in section 4 show that the characteristic phenomenon in the strong perturbation regime, i.e. the fringed tunnelling, occurs in the asymptotic region of the transmissive side, and it is attributed to the interference of the multiple branches, each of which belongs to a different critical point. Hence, if we wish to understand the underlying mechanism of the fringed tunnelling including the asymptotic region, we have to take into account the global structure of the $\mathcal{L}$-set far from the scattering

region by extending the subset $\mathcal{M}_c$ to the outside of the characteristic neighbourhood $B(t_2)$. It should be noted that, in section 5.2, the existence of $\mathcal{M}_c$ was proven only in $B(t_2)$, but it is really possible to extend our low-frequency analyses naturally to the asymptotic region and to prove the existence of $\mathcal{M}_c$ extended to the asymptotic region. Since a detailed description of analyses in the asymptotic region will take up much space and we cannot afford to elaborate on it in this paper, this will be published in a subsequent paper [36].

Here, we simply suppose that $\mathcal{M}_c$ is naturally extended to the outside of $B(t_2)$ and the corresponding $\mathcal{L}$-set transverses from one asymptotic side (the transmissive side) to the other (the reflective side).

5.4.1. Rapid approach of tunnelling trajectories towards real phase plane. First of all, we consider in more detail how the trajectories starting at $\mathcal{M}_c$ in $B(t_2)$ travel in the complex phase space. Then, we suppose, for a while, that initial points of trajectories are in $B(t_2)$. From the discussion of section 5.3, if the lapse time is sufficient large, i.e. $t_2 - \mathrm{Re}\ \mu_{-c} \gg 1$, the radius of $B(t_2)$ becomes extremely small (equation (5.55)), and then the parameter α of the trajectory with $t_1 \in B(t_2)$ can be taken exponentially small.

Then as is shown in section 5.2.5, $\mathrm{Re}\,\mu_- \ll t_2 < \mathrm{Re}\,\mu_+$, and we can choose the time path in such a way that it is on the real axis if $\mathrm{Re}\,\mu_- < \mathrm{Re}\,t\,(<t_2)$. In equations (5.44) and (5.45), the phase $\varphi(t)$ is expressed by equation (5.50), and the first term $\sim |\alpha^2\,\mathrm{e}^{\varphi}| \sim |\alpha^2|\,\mathrm{e}^{\mathrm{Re}\,\varphi}$ is much less than the second term $\sim |\mathrm{e}^{-\varphi}| = \mathrm{e}^{-\mathrm{Re}\,\varphi}$ if $\mathrm{Re}\,t$ is not much larger than $\mathrm{Re}\,\mu_-$. Then the trajectory with $t_1 \in B(t_2)$ traces a particular trajectory on the stable manifold, which starts at $t = t_{1c}$ and is given by setting $\alpha = 0$, namely,

$$(Q(t), P(t)) = (\sinh^{-1}\{\mathrm{e}^{-\varphi(t)}\}, -\mathrm{sech}\,Q(t)\sqrt{2a(t)}\,\mathrm{e}^{-\varphi(t)}) \tag{5.59}$$

until the time $t_M \in \mathbf{R}$ at which the first term balances with the second term, i.e. $\mathrm{e}^{-\mathrm{Re}\,\varphi(t_M)} \sim |\alpha|$. At $t = t_M$, the trajectory passes close to the unstable fixed point O at distance of $O(|\alpha|)$ from it, and beyond t_M the first term of equation (5.44) (and equation (5.45)) explodes exponentially and dominates the second term which decreases exponentially. This means that the distance from a point on the trajectory to the (complexified) unstable manifold decreases exponentially with the increase in the lapse time; this is just the extension of the so-called lambda lemma to the complex domain, which has been proven for the real-domain dynamics [35].

Consequently, the tunnelling trajectory has a remarkable characteristic that it swings across the scattering region guided by the stable and unstable manifolds. We next focus our attention on the itinerary of the tunnelling trajectory through the complex domain of the phase space. Taking into account the output boundary condition as well as the relation (5.52), equation (5.44) is rewritten as

$$\begin{aligned} &\sinh Q = f_1(t) + f_2(t) \quad \text{where} \\ &f_1(t) = \sqrt{a(t_2)/a(t)}(Y - \mathrm{e}^{-\varphi_2})\,\mathrm{e}^{\Delta\varphi(t)} \quad f_2(t) = \mathrm{e}^{-\varphi_2}\,\mathrm{e}^{-\Delta\varphi(t)} \end{aligned} \tag{5.60}$$

where $\varphi_2 \equiv \varphi(t_2) \sim \nu(t_2 - \mu_-) \sim -2\,\log\,\alpha$, and

$$\Delta\varphi(t) \equiv \int_{t_2}^{t} \mathrm{d}s\sqrt{2a(s)} + \log\{a(t)/a(t_2)\}/4 \sim \nu(t - t_2) \tag{5.61}$$

is real-valued because of our choice of the time path. Thus, in equation (5.60) all the parameters except $\mathrm{e}^{\pm\varphi_2}$ are real numbers. For $t \sim \mathrm{Re}\,\mu_-(\ll t_M)$, the second term f_2, which has an appreciable amount of imaginary components, is much larger than the first term f_1, but it decays exponentially with an increase in t. As t exceeds t_M, f_2 is overwhelmed by f_1, which grows exponentially as $\mathrm{e}^{\Delta\varphi(t)}$. But f_1 always has a very small imaginary component less than

$e^{-\mathrm{Re}\,\varphi_2}$, while the imaginary component of f_2 is also very small and is less than $O(e^{-\mathrm{Re}\,\varphi_2/2})$ for $t > t_M$. It is not difficult to show that $P(t)(=\dot{Q}(t))$ also exhibits the same behaviour.

Summarizing the above arguments, the tunnelling trajectory, which once moves into the complex domain of the phase space, approaches the real phase plane very rapidly guided by the CSM of the unstable fixed point O and after that it moves close to the real plane sticking to the unstable manifold of O. The major part of the imaginary component of the trajectory for $\mathrm{Re}\,t < t_M$ arises from its stable component, $e^{-\varphi}(= f_2)$, which is, except for small corrections of $O(\alpha^2)$, identified with that of the characteristic trajectory on the stable manifold given by equation (5.59).

It should be emphasized that the remarkable role played by the stable and unstable manifolds in the tunnelling process is common even in more complicated situations of chaotic tunnelling, which can be dealt with only by quantum map models [17]. The set of tunnelling trajectories rapidly approaching toward the chaotic real phase plane plays a predominant role in chaotic tunnelling of quantum maps and it has a profound relationship with the Julia set, the key concept in the theory of complex dynamical systems [18]. The present case does not treat such an actually complicated situation of chaos, but it provides the 'minimal' model of intrinsically chaotic systems which allows detailed analytical studies.

5.4.2. Appearance of an infinite number of possibly contributing tunnelling trajectories. From the above arguments together with those in section 5.3, the end point (Q_2, P_2) transverse the phase space from the transmissive side to the reflective side (and vice versa) along the real unstable manifold as t_1 is moved along $\mathcal{M}_c$. Indeed, if we set $Q_2 \in \mathbf{R}$ in the scattering region at a given $t = t_2(\in \mathbf{R})$, then $\mathrm{Im}\,P_2$ is estimated from equations (5.58) and (5.50) as

$$\mathrm{Im}\,P_2 = -\mathrm{Im}\,C_1\,\mathrm{sech}Q_2 \sim O(\exp(-\nu(t_2 - \mathrm{Re}\,\mu_{-c}))) \tag{5.62}$$

which means that the imaginary part of P_2 decreases exponentially in the limit of $\mathrm{Re}\,s(= t_2 - \mathrm{Re}\,t_1) \to \infty$. Therefore, the $\mathcal{L}$-set transverses the phase space along the real unstable manifold at least in the scattering region, and it is also natural to suppose that the $\mathcal{L}$-set follows the real unstable manifolds in both asymptotic sides to a certain extent [36].

Now, let us consider the following problem: why and how do the characteristic sets $\mathcal{M}_c$, each of which passes close to a different critical point, simultaneously contribute to the fringed tunnelling? Remember that the critical points appear periodically in the initial time plane t_1 due to the periodicity of the perturbation, and so do $\mathcal{M}_c$ each associated with a different critical point (see figure 8(a)). As a result, there exist, in the phase space, an infinite number of branches of the $\mathcal{L}$-set each corresponding to a different $\mathcal{M}_c$ (see figure 8(b)). All of them intersect with the observatory line $Q = Q_2$ in the phase space and contribute to the tunnelling probability.

The intersection of the stable manifold with the incident beam set takes place in the complex phase space at an arbitrary perturbation strength ϵ. As ϵ increases and exceeds ϵ_{th} (see section 5.1), the complex intersection represented by t_{1c} reaches the real phase plane, and a complicated *heteroclinic-like entanglement* between two different sorts of the invariant sets, namely, the stable manifold and the incident beam set (which is extended to the scattering region), should emerge in the *real* phase space, which is a common situation in nonintegrable scattered-reaction systems [37, 38]. However, it should be emphasized that the entanglement between the two objects is taking place at an arbitrary perturbation strength in the complexified phase space, and the appearance of multiply coexisting branches of the $\mathcal{L}$-set demonstrated in the above paragraph is just the manifestation of the *heteroclinic-like entanglement* in the complex domain.

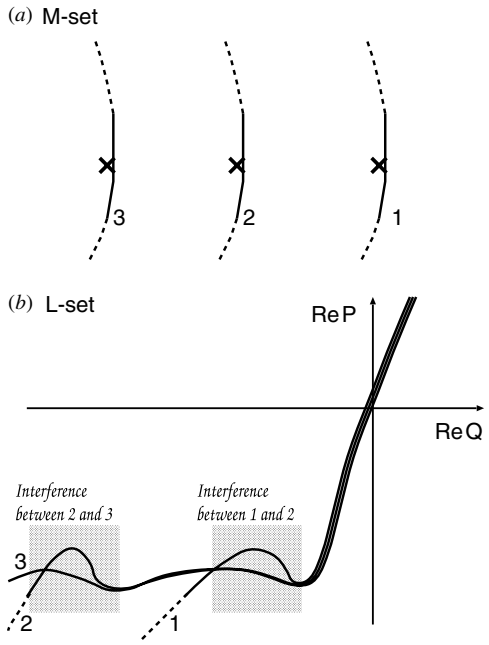

Figure 8. A sketch of how multiple branches contribute to the interference fringe. (*a*) Periodicity of critical points in t_1 plane, each of which is accompanied by a branch passing close to it. (*b*) The branches in the $\mathcal{L}$-set. The fringed patterns are created by the interference of the branches in the hatched regions.

5.4.3. Actual contribution from multiple tunnelling trajectories. Given t_2 and Q_2, an infinite number of trajectories can contribute to the semiclassical wave-matrix (2.3). Based upon the remarkable features of the trajectories approaching the real plane guided by the stable manifold, we can show that Im S_Ω of each trajectory, which is the primary factor controlling the extent of contribution to the wave-matrix, is almost the same.

Let us denote the set $\mathcal{M}_c$ close to the nth critical point $t_{1c}^{(n)} = t_{1c}^{(0)} - nT\,(n \in \mathbf{N})$ by $\mathcal{M}_c^{(n)}$, where $t_{1c}^{(0)}$ is a properly chosen critical point. The superscript $^{(n)}$ is used to denote explicitly the assignment to $t_{1c}^{(n)}$. Because of the periodicity of the perturbation, if the same integration path is taken, all the characteristic trajectories starting at $t_{1c}^{(n)}$ have the same form as the function of the lapse time s independent of n. Then, except for the correction of $O(|\alpha^{(n)}|^2) \ll 1$, every trajectory initially at $t_1 \in \mathcal{M}_c^{(n)}$ traces the same itinerary (i.e. the characteristic trajectory (5.59)) in the complex phase space independent of n, until it approaches the real plane. Furthermore, most of the imaginary component of the trajectory is carried by its stable component $\mathrm{e}^{-\varphi}$, which is substantially identified with that of the characteristic trajectory (5.59). Therefore, Im S_Ω is evaluated by substituting equation (5.59) into equation (2.6).

As a result, Im $S_\Omega^{(n)}$ is almost the same for all the trajectories started at $t_1 \in \mathcal{M}_c^{(n)}$, whereas Re $S_\Omega^{(n)}$ may be significantly different reflecting the difference in the itinerary after approaching close to the real plane, which is represented by $f_1(t)$ in equation (5.60), or the first terms of equations (5.44) and (5.45). The contribution from $\mathcal{M}_c^{(n)}$ is, therefore, decided by the *classical* amplitude factor

$$|\partial^2 S_\Omega / \partial E_1 \partial Q_2|^{1/2} = |\partial Q_2(t_2, t_1, P_1, Q_1)/\partial t_1|^{-1/2} \tag{5.63}$$

which is considered as the secondary factor in the ordinary situation of the tunnelling process. The right-hand side tells us that Q must be known as a function of initial condition including t_1. Returning to equation (5.51), we immediately obtain

$$|\partial Q(t_2 - t_1, t_1, Q_1, P_1)/\partial t_1|^{-1} = |4\sqrt{2a(t_2)}\,\cosh(Q_2)\,\mathrm{e}^{-\varphi(T_2)}/A_1|. \tag{5.64}$$

For large n, the amplitude factor decays exponentially as $|\partial^2 S_\Omega/\partial E_1 \partial Q_2|^{1/2} \propto \mathrm{e}^{-nT/2}$. Consequently, among an infinite number of the possibly contributing tunnelling trajectories, only the finite number of $\mathcal{M}_c^{(n)}$ with relatively small n actually contribute to the tunnelling probability at Q_2 (see figure 8(*b*)). All the claims presented above are obtained supposing that Q_2 is in the scattering region, but they all hold correct even in the asymptotic region [36].

As shown in figure 4, the interference of the characteristic branches **1** and **2** makes the fringed pattern in the region A, while branch **5** together with branches **3** and **4**, which are bifurcated from branch **2** in time evolution, contributes in the region B. Hence, it is confirmed that the branches associated with the critical points have a significant effect on the construction of the fringed pattern, and we come to a complete understanding of underlying mechanism of the fringed tunnelling.

5.4.4. Characteristic perturbation strength. The most important fact is that the tunnelling mechanism in the regime of the perturbation strength strong enough to yield the fringed tunnelling is quite different from the (perturbed) instanton mechanism of the tunnelling in the weak perturbation regime [19, 20]. We discuss here how the transition of the tunnelling mechanism occurs as the perturbation strength is increased.

As was stressed in section 5.1, there always exist the critical points t_{1c}, even if the strength of the perturbation is arbitrarily small. Such critical points, however, have a large imaginary component and are located so deeply in the imaginary domain of the complex plane that they do not affect the dominating instanton branches associated with the integration path C_1. As the perturbation increases, the imaginary component of the critical points decreases and they finally go across the dominant branches with the path C_1. This is the case that the structure of the branches are broken up and reconstructed by the influence of the critical points.

Using the above criterion, it is possible to estimate the characteristic value of the perturbation strength, above which the critical point significantly influences the dominant branches and results in the fringed tunnelling. The imaginary depth of the dominant branches of the $\mathcal{M}$-set is roughly estimated as $|\mathrm{Im}(t_2 - t_1)| \sim \pi/\nu$. Therefore, the characteristic value $\epsilon = \epsilon_c$ is the value at which the critical point t_{1c} passing through the border of the Riemann sheets of the dominant and next-order branches, whose imaginary depth is estimated as $\sim 3\pi/2\nu$:

$$|\mathrm{Im}\, t_{1c}| \sim 3\pi/2\nu. \tag{5.65}$$

Substituting the estimation of $\mathrm{Im}\, t_{1c}$ by the Melnikov method (equation (5.13)) into equation (5.65) and setting $\nu \sim \sqrt{2}$, we obtain the characteristic perturbation strength

$$\epsilon_c \sim (1 - E_1)/\{(1 - \chi(\omega))\cosh(3\omega\pi/2\sqrt{2})\} \tag{5.66}$$

above which the fringed tunnelling may be observed. In other words, if ϵ is given, the fringed tunnelling is observed above the characteristic energy

$$E_{1c} = 1 - \epsilon\{(1 - \chi(\omega))\cosh(3\omega\pi/2\sqrt{2})\}. \tag{5.67}$$

Sufficiently below it the 1D instanton picture works well.

Finally, we compare in figure 9 the above theoretical value of ϵ_c with the numerically decided characteristic perturbation strength above which the tunnelling component exhibits a definite fringed pattern. The numerical ϵ_c is decided at three relatively small ω. The agreement of the theory with the numerical data seems to be satisfactory.

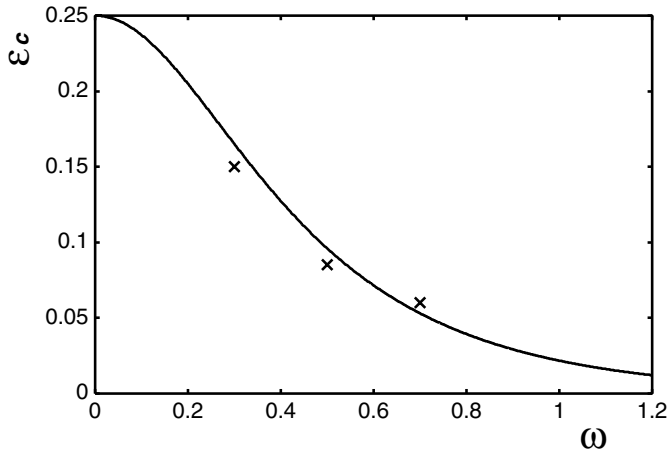

Figure 9. The characteristic strength ϵ versus ω. The solid line indicates the theoretical estimate of the characteristic strength ϵ_c as a function of ω, while the values of ϵ_c which are numerically decided at three relatively small ω are marked by $\times$.

6. Summary and remarks

The fringed tunnelling, which is observed in 1.5D barrier systems (i.e. periodically driven 1D barrier systems) and in autonomous 2D barrier systems as well, is regarded as a manifestation of an intrinsic effect of multi-dimensionality on the tunnelling process. Semiclassical interpretation of it is successfully attained by taking into account the contribution of multiple tunnelling trajectories whose character is very different from that of the tunnelling trajectory such as the instanton of the unperturbed system.

In this paper, we have developed theoretical analyses, which provide us with a complete understanding of the hidden *classical* origin behind that simultaneous contribution of multiple tunnelling trajectories, which is directly reflected in the formation of the interference fringe on the tunnelling wavefunction. The key object in the analyses is the critical point t_{1c}, at which the divergent movement of the singularities of the trajectory occurs. It is just the intersection of the CSM and the incident beam set, i.e. the *heteroclinic-like entanglement* between the complexified invariant sets.

The analyses in section 5 are the central part of the present paper, which elucidates the classical mechanism in the creation of multiple contributing branches by the influence of the critical points. Previous to this section, we introduced the basic tools such as the $\mathcal{M}$-set (the set of initial conditions of the contributing trajectories) and the $\mathcal{L}$-set (the Lagrangian manifold), and discussed the complexified classical dynamics of the unperturbed system. In section 5, we started our analysis by using the Melnikov method, and showed that the trajectory starting at the critical point is of a solution of the CSM. Indeed, the critical point is an intersection between the CSM and the initial time plane t_1, and such intersections appear periodically due to the periodicity of the perturbation. Next, we introduced a solution in the low-frequency limit that allowed us to investigate the characteristics of the critical point and of the branch associated with it. If we take an initial time close to t_{1c}, the group of singularities Sg_n^+ diverges as $Sg_n^+ \sim -\log(t_1 - t_{1c})/\nu$, and we always find that the set $\mathcal{M}_c$, a subset of $\mathcal{M}$, forms a line passing very close to t_{1c}. Furthermore, as t_1 is moved along $\mathcal{M}_c$, switching of the path-topology is induced by the divergent-detouring behaviour of the singularities Sg_n^+, and the end point of the trajectory $(Q(t_2 - t_1, t_1), P(t_2 - t_1, t_1))$ traverses continuously but abruptly from

the transmissive side to reflective side (and vice versa) passing close to the unstable fixed point (or the unstable periodic orbit) at the origin. This means that such an $\mathcal{M}_c$ forms a merged object in the $\mathcal{L}$-set connecting to both transmissive and reflective sides with following the unstable manifold.

The results of the analyses provide us with a comprehensive understanding of the local structure near the critical point; in terms of the $\mathcal{L}$-set, the structure of the branches fully inside the scattering region.

Furthermore, it is natural to assume that such a characteristic branch in the $\mathcal{L}$-set is extended into the asymptotic regions in both transmissive and reflective sides following the unstable manifold. Since the periodicity of the perturbation creates an infinite number of the critical points each accompanied by a corresponding characteristic branch, then an infinite number of characteristic branches following the unstable manifold appear. And some of these contribute to the tunnelling probability, and their interference results in the fringed pattern. Such a structure of the branches reminds us of the complexified *heteroclinic-like entanglement*; the incident beam set $\mathcal{I}$ entangled with the CSM is mapped to a surface that is multiply folded in the scattering region piling up on the unstable manifold and being extended along it, and the characteristic branches are just subsets of the mapped surface of $\mathcal{I}$ that satisfy the output-boundary condition of the wave-matrix.

However, if we wish to more completely understand the underlying mechanism of the fringed tunnelling, we have to develop an analysis working on the fully asymptotic region, which naturally leads to the S-matrix theory. Full details concerning the subject will be published in a forthcoming paper [36].

The character of trajectories contributing to the fringed tunnelling is essentially different from that of the instanton picture. In application of the 1D instanton theory to a multi-dimensional system, we have to assume that the system is integrable, and the tunnelling trajectory running in the complexified phase space follows the complexified invariant surface of the integrable system, i.e. the complexified KAM torus [9], although it is not the case even for nearly integrable systems. Indeed, the KAM tori are in general interrupted by a natural boundary [39]. On the other hand, the trajectories contributing to the fringed tunnelling are guided by the CSM from the beginning, thereby approaching the real plane by the attraction of the unstable fixed point (generally unstable periodic orbit). After that the trajectory is repelled by the fixed point and travels very close to the real plane, being scattered toward the asymptotic region along the unstable manifold.

It is recognized that such a characteristic dynamical process is commonly observed in the chaotic tunnelling process of quantum maps [17, 18]. The quantum map has no continuous time and so has no counterparts of the time singularity and of the critical point as well. It is surprising that, in spite of such a marked difference in the mathematical nature of models, the physical interpretation of the tunnelling process seems to provide a common picture, at least on the phenomenological level. Unfortunately, however, the mathematical structure of the tunnelling mechanism including the relationship with the traditional view of the instanton, which is the major subject of this paper, is very unclear in the quantum map models because of the absence of the key concept corresponding to the time singularity. Instead, the presence of a complex-domain chaos and its relationship to the predominant tunnelling trajectories are clarified by using the Gaussian map [17]. The chaotic dynamical structure underlying the new tunnelling mechanism is the issue that still remains inaccessible by the continuous time system.

The complexified *heteroclinic-like entanglement* between the incident beam set and the CSM makes the tunnelling path stick to the complexified stable and unstable manifolds, which form basic geometrical structures creating the chaotic complexity in the phase space

in multi-dimensional systems. The appearance of such a *heteroclinic-like entanglement* in the complex domain seems to be quite generic in multi-dimensional systems, and the fringed tunnelling is numerically observed in the autonomous multi-dimensional barrier tunnelling process [21, 22, 24]. It is safe to say that the classical mechanism which has been clarified in this paper provides us with a clue to a generic understanding of influence of the complexity of complexified classical chaos on the tunnelling process observed in multi-dimensional systems.

Acknowledgments

The authors are very grateful to A Shudo, T Onishi and A Yoshimoto for valuable discussions and comments. One of the authors (KT) is very grateful to A Voros and his colleagues for the warm hospitality received at CEA-Saclay, where half of this paper was written. The authors express thanks to S Tsuji for his hospitality in providing a location for our discussions, where some important progress in the idea of the present work was made. The present work was supported by Grant-in-Aid for Scientific Research (C) No 13640410, from the Japan Society for the Promotion of Science (JSPA) and Grant-in-Aid for Scientific Research on Priority Areas(2) No 14077220 from the Ministry of Education, Culture, Sports, Science and Technology.

Appendix A. On adiabatic solutions

We first decide the explicit functional form of $E(t)$ by integrating the energy gain equation (5.19) over t. Then it is more convenient to use ϕ as the integration variable instead of t. The relation $\phi(t) = \int_{t_0}^{t} \mathrm{d}t' \sqrt{2E(t')}$ (equation (5.17)) implies that ϕ can be made as a single valued function of t. (Even in the scattering region the major part of $\phi(t)$ varies linearly as $\phi(t) \sim \sqrt{2E(t_0)}(t - t_0)$, because $E(t)$ varies slowly in time.) When we regard a function $F(t)$ as a function of ϕ in place of t, we denote it simply by $F(\phi)$.

By using the definition of the gates $\mu_{\pm}$ given by equation (5.24), we obtain

$$\mathrm{e}^{\mp 2\phi_{\mp}} = 4\{1 + r(t)^2/2 + O(r^4)\}/r(t)^2|_{t=\mp\mu} \tag{A.1}$$

where $\phi_{\mp} = \phi(t = \mu_{\mp})$ and very small terms such as $\frac{\mathrm{d}}{\mathrm{d}t} r(t)^2 \sim O(\alpha^2\omega\epsilon)$, which is estimated from equations (5.18) and (5.19), are neglected. The function h introduced by equation (5.20) can be approximated by

$$\begin{aligned} h(\phi) &= \{1 + r^2/2 + r^2/4\,\mathrm{e}^{\mp 2\phi} + O(r^4)\}^{-1} \\ &= \{(1 + r^2/2)[1 + \mathrm{e}^{\mp 2(\phi - \phi_{\mp})}]\}^{-1} + O(r^4) \end{aligned} \tag{A.2}$$

in the vicinity of $t = \mu_{\mp}$ or $\phi_{\mp} = \phi(\mu_{\mp})$.

Equation (A.2) indicates that $h(\phi)$ increases abruptly from 0 to $1/(1 + r^2)$ at μ_{-} and decreases from $1/(1 + r^2)$ to zero at μ_{+} (see figure 6(b)), if the integration path is taken so as to be parallel with the real axis in the vicinities of $\mu_{\mp}$ as shown in figure 6(a). Therefore, its derivative $\mathrm{d}h(\phi)/\mathrm{d}\phi$ is close to zero except in the vicinities of $\mu_{\mp}$, where it has a sharp peak or valley (see figure 6(c)). We multiply $\frac{\mathrm{d}h}{\mathrm{d}\phi}$ by a slowly varying function such as $a(t)$ or $a(\phi)$ and integrate it along the integration path from $\phi = 0$ in the direction of $\mathrm{Re}\{\phi\}$ increasing (the forward direction). Then we expand the slowly varying function $a(\phi)$ into the Taylor series (it is an expansion with respect to ω) at $\min_R(\phi, \phi_{+})$ where the absolute value of the

integrand $\left|a\frac{\mathrm{d}h}{\mathrm{d}\phi}\right|$ has a sharp maximum in the range of integration, and retain only the lowest order expansion term with respect to ω,

$$\int_0^{\phi}\frac{\mathrm{d}h(\phi')}{\mathrm{d}\phi'}a(\phi')\,\mathrm{d}\phi' = a(\min_R\{\phi,\phi_+\})\int_0^{\phi}\frac{\mathrm{d}h(\phi')}{\mathrm{d}\phi'}\,\mathrm{d}\phi' + \text{correction} \tag{A.3}$$

where the correction is estimated by the second lowest order term of the Taylor expansion of the slowly varying function at $\min_R\{\phi,\phi_+\}$

$$|\text{correction}| \sim \left|\frac{\mathrm{d}a(\phi)}{\mathrm{d}\phi}\right|_{\phi=\min_R\{\phi,\phi_+\}}\int_0^{\phi}\left|(\phi-\phi')\frac{\mathrm{d}h(\phi')}{\mathrm{d}\phi'}\right|\mathrm{d}\phi' \sim O(\epsilon\omega) \ll 1 \tag{A.4}$$

and $\min_R$ is defined by equation (5.26). The integration of equation (5.19) in the forward (i.e. $\mathrm{Re}\,\phi$ increases) yields

$$\begin{aligned} E(t)-E(t_0) &= \int_{t_0}^{t}\mathrm{d}t'\frac{\dot{a}(t')}{1+r^2(t')\cosh^2\phi(t')} = \int_0^{\phi}\mathrm{d}\phi'\frac{\mathrm{d}a(\phi')}{\mathrm{d}\phi'}h(\phi') \\ &= a(\phi')h(\phi')|_{\phi'=0}^{\phi'=\phi} - \int_0^{\phi}d\phi' a(\phi')\frac{\mathrm{d}h(\phi')}{\mathrm{d}\phi'} \end{aligned} \tag{A.5}$$

and so it is approximated up to the correction of $O(\epsilon\omega)$ by using equation (A.3)

$$E(t) = a(t)h(t) - a(\min_R\{t,\mu_+\})(h(t)-h(t_0)) + O(\epsilon\omega). \tag{A.6}$$

Here the relation $a(\phi=0)h(\phi=0) = a(t_0)h(t_0) = E(t_0)$ is used.

Omitting the correction of $O(\epsilon\omega)$, the integration forward ($\mathrm{Re}\{t\}$ increases) immediately yields equation (5.28) for $t_0 \leqslant t \leqslant \mu_+$. For $t \geqslant \mu_+$, on the other hand, we obtain

$$\phi(t) = \phi(\mu_+) + \int_{\mu_+}^{t}\mathrm{d}t'\sqrt{2a(\mu_+)h(t_0)} + \delta\phi(t). \tag{A.7}$$

Note that $\phi(\mu_+) = \int_{t_0}^{\mu+}\mathrm{d}t'\sqrt{2a(t')h(t_0)}$ (equation (5.28)), and the last term defined by

$$\delta\phi(t) = \int_{\mu_+}^{t}\mathrm{d}t'\left\{\sqrt{2[a(t')h(t') - a(\mu_+)(h(t')-h(t_0))]} - \sqrt{2a(\mu_+)h(t_0)}\right\} \tag{A.8}$$

gives the correction of $O(\epsilon\omega)$, because it is estimated as

$$\begin{aligned} &\int_{\mu_+}^{t}\frac{2[a(t')h(t') - a(\mu_+)h(t')]}{\sqrt{2[a(t')h(t') - a(\mu_+)(h(t')-h(t_0))]} + \sqrt{2a(\mu_+)h(t_0)}}\,\mathrm{d}t' \\ &\qquad \sim \int_{\mu_+}^{t}[a(t')h(t') - a(\mu_+)h(t')]\,\mathrm{d}t' \sim \int_{\mu_+}^{t}[\dot{a}(\mu_+)(t'-\mu_+)h(t')]\,\mathrm{d}t' \sim O(\epsilon\omega). \end{aligned}$$

Omitting this correction, we obtain equation (5.29). By the same manner, the integration backward gives equation (5.27)

Appendix B. On singularities of perturbed system

The singularity t_{sg} is the time at which the potential diverges, and so it is the zero of the denominator of $h(t)$ (see equation (5.20)), namely

$$r(t_{sg})\cosh\phi(t_{sg}) = \pm\mathrm{i} \qquad \text{or approximately} \qquad r(t_{sg})\,\mathrm{e}^{\pm\phi(t_{sg})}/2 = \pm\mathrm{i} \tag{B.1}$$

in the limit of $|\alpha^2| \ll 1$. t_{sg} is not far from the gates $\mu_\pm$ satisfying equation (5.35):

$$r(\mu_\pm)\,\mathrm{e}^{\pm\phi(\mu_\pm)}/2 = \pm 1 + O(r^2). \tag{B.2}$$

In terms of the phase variable the difference is

$$\phi(t_{sg}) - \phi(\mu_\pm) = \pm(\pm\mathrm{i}\pi/2 + \log(r(\mu_\pm)/r(t_{sg}))) \tag{B.3}$$

and it is convenient to suppose a path from $\phi_\pm = \phi(\mu_\pm)$ to $\phi_{sg} = \phi(t_{sg})$ in the ϕ-space. A noteworthy fact is that the energy gained along the path diverges logarithmically. Indeed,

$$\begin{aligned} E - E(\mu_+) &= \int_{\phi_+}^{\phi} \frac{\mathrm{d}a(\phi')}{\mathrm{d}\phi'} h(\phi')\,\mathrm{d}\phi' \\ &\sim \frac{\mathrm{d}a(\phi_+)}{\mathrm{d}\phi_+} \int_0^{\phi-\phi_+} \frac{1}{1+\mathrm{e}^{2x}}\,\mathrm{d}x \\ &= \frac{1}{2}\frac{\mathrm{d}a(\phi_+)}{\mathrm{d}\phi_+}[x - \log\{\cosh x\}]|_{x=0}^{x=\phi-\phi_+}. \end{aligned} \tag{B.4}$$

Using this result in the phase equation (5.17), we obtain

$$t_{sg} - \mu_+ \sim \int_0^{\pm\mathrm{i}\pi/2} \frac{\mathrm{d}z}{\sqrt{2E(\mu_+) + a(\phi_+)'(z - \log\{\cosh z\})}} \qquad \left(a(\phi_+)' \equiv \frac{\mathrm{d}a(\phi_+)}{\mathrm{d}\phi_+}\right). \tag{B.5}$$

Considering that $|a(\phi_+)'/E(\mu_+)| \sim \epsilon\omega \ll 1$, it is easy to show that

$$|t_{sg} - \mu_+| = \frac{1}{\sqrt{|a(\phi_+)'|}} \int_0^{\pm\pi/2} \mathrm{d}x\{(R_1 - \log\{\cos x\})^2 + (R_2 - x)^2]\}^{-1/4} \tag{B.6}$$

where R_1 and R_2 are certain constants. It can easily be proven to be less than a certain constant

$$|t_{sg} - \mu_+| < M/\sqrt{|E(\mu_+)|} \tag{B.7}$$

where $M(>0)$ is a certain numerical constant.

References

[1] Keller J B 1958 'The Geometrical Theory of Diffraction' in The American Mathematical Society *Calculus of Variations and Its Applications* (New York: McGraw-Hill)
Keller J B 1958 *Proc. Symp. Appl. Math.* **8** 27
Seckler B and Keller J B 1959 *J. Acoust. Soc. Am.* **31** 192
Patashinskii A Z, Pokrovskii V L and Khalatnikov I M 1963 *Sov. Phys.–JETP* **17** 1387
Patashinskii A Z, Pokrovskii V L and Khalatnikov I M 1964 *Sov. Phys.–JETP* **18** 522
Patashinskii A Z, Pokrovskii V L and Khalatnikov I M 1964 *Sov. Phys.–JETP* **18** 683
Maslov V P 1964 *Sov. Phys. Dokl.* **6** 666

[2] Schulman L S 1981 *Techinques and Applications of Path Integration* (New York: Wiley)

[3] Benderskii V A, Makarov D E and Wight C A 1994 *Adv. Chem. Phys.* **88** 1
Marcus R A and Coltrin M E 1977 *J. Chem. Phys.* **67** 2609
Garrett B C, Truhlar D G, Wagner A F and Dunning T H Jr 1983 *J. Chem. Phys.* **78** 4400
Truhlar D G, Isaacson A D, Skodje R T and Garrett B C 1982 *J. Phys. Chem.* **86** 2252
Shida N, Barbara P F and Almlof J 1989 *J. Chem. Phys.* **91** 4061
Shida N, Barbara P F and Almlof J 1991 *J. Chem. Phys.* **94** 3633
Shida N, Barbara P F and Almlof J 1991 *J. Chem. Phys.* **95** 10457
Miller W H, Ruf B A and Chang Y-T 1988 *J. Chem. Phys.* **89** 6298

[4] Knoll J and Schaeffer R 1976 *Ann. Phys., NY* **97** 307

[5] Balian R and Bloch C 1974 *Ann. Phys., NY* **85** 514

[6] Voros A 1983 *Ann. Inst. H Poincaré* **39** 211
Voros A 1994 *J. Phys. A: Math. Gen.* **27** 4653
Voros A 2000 *J. Phys. A: Math. Gen.* **33** 7423

[7] Miller W H and George T F 1972 *J. Chem. Phys.* **56** 5668
George T F and Miller W H 1972 *J. Chem. Phys.* **57** 2458

[8] Miller W H 1970 *J. Chem. Phys,* **53** 1949
Miller W H 1974 *Adv. Chem. Phys.* **25** 69

[9] Wilkinson M 1986 *Physica* D **21** 341
Wilkinson M and Hannay J H 1987 *Physica* D **27** 201

[10] Gutzwiller M C 1967 *J. Math. Phys.* **8** 1979
Gutzwiller M C 1969 *J. Math. Phys.* **10** 1004
Gutzwiller M C 1970 *J. Math. Phys.* **11** 1791
Gutzwiller M C 1971 *J. Math. Phys.* **12** 343
Gutzwiller M C 1973 *J. Math. Phys.* **14** 139
Gutzwiller M C 1977 *J. Math. Phys.* **18** 806
[11] Gutzwiller M C 1990 *Chaos in Classical and Quantum Mechanics* (New York: Springer)
[12] Bohigas O, Tomsovic S and Ullmo D 1990 *Phys. Rev. Lett.* **65** 5
Bohigas O, Tomsovic S and Ullmo D 1993 *Phys. Rep.* **223** 45
Bohigas O, Egydo de Carvalho R and Marvulle V 1993 *Nucl. Phys.* A **560** 197
Leyvraz F and Ullmo D 1996 *J. Phys. A: Math. Gen.* **29** 2529
Brodier O, Schlagheck P and Ullmo D 2001 *Phys. Rev. Lett.* **87** 064101
Brodier O, Schlagheck P and Ullmo D 2002 *Ann. Phys., NY* **300** 88
Creagh S C and Whelan N D 1999 *Ann. Phys., NY* **272** 196
Creagh S C and Whelan N D 2000 *Phys. Rev. Lett.* **84** 4084
Creagh S C, Lee S Y and Whelan N D 2002 *Ann. Phys., NY* **295** 194
Bies W E, Kaplan L and Heller E J 2001 *Phys. Rev.* E **64** 016204
[13] Creagh S C 1998 *Tunnelling in Two Dimensions in Tunnelling in Complex Systems* ed S Tomsovic (Singapore: World Scientific) pp 35–100
[14] Steck D A, Oskay W H and Raizen M G 2001 *Science* **293** 274
Hensinger W K, Haffer H, Browaeys A, Heckenberg N R, Helmerson K, McKenzie C, Milburn G J, Phillips W D, Rolston S L, Rubinsztein-Dunlop H and Upcroft B 2001 *Nature* **412** 52
[15] Creagh S C and Whelan N D 1996 *Phys. Rev. Lett.* **77** 4975
Creagh S C and Whelan N D 1999 *Phys. Rev. Lett.* **82** 5237
[16] Shudo A and Ikeda K S 1995 *Phys. Rev. Lett.* **74** 682
Shudo A and Ikeda K S 1998 *Physica* D **115** 234
[17] Onishi T, Shudo A, Ikeda K S and Takahashi K 2001 *Phys. Rev.* E **64** 025201
Onishi T, Shudo A, Ikeda K S and Takahashi K 2003 Semiclassical study on tunnelling processes via complex-domain chaos *Preprint* nlin.CD/0301004
[18] Shudo A, Ishii Y and Ikeda K S 2002 *J. Phys. A: Math. Gen.* **35** L225 (see also forthcoming publications)
[19] Takahashi K and Ikeda K S 2000 *Ann. Phys., NY* **283** 94
[20] Takahashi K and Ikeda K S 2001 *Found. Phys.* **31** 177
[21] Takahashi K, Yoshimoto A and Ikeda K S 2002 *Phys. Lett.* A **297** 370
[22] Takahashi K and Ikeda K S 2003 Complex-domain semiclassical theory and periodically perturbed barrier tunnelling problems *J. Phys. Soc. Jpn. suppl.* at press
[23] Floquet G 1883 *Ann. Ec. Norm. Suppl.* **12** 47
Sambe H 1973 *Phys. Rev.* A **207** 315
Howland J S 1974 *Math. Ann.* **207** 315
[24] Yoshimoto A 2000 *Rep. Math. Phys.* **46** 303
[25] See, for example, Ramani A, Grammaticos B and Bountis T 1989 *Phys. Rep.* **180** 159–245, and references therein
[26] Goriely A and Tabor M 1995 *Physica* D **85** 93
[27] Newton R G 1982 *Scattering Theory of Waves and Particles* 2nd edn (New York: Springer)
[28] Takahashi K and Ikeda K S 1997 *J. Chem. Phys.* **106** 4463
[29] Stokes G G 1864 *Trans. Cambridge Phil. Soc.* **10** 106
Dingle R B 1973 *Asymptotic Expansions: Their Derivation and Interpretation* (London: Academic)
For a very recent development on the study of Stokes phenomenon, see, for example Sternin B Y and Shatalov V E 1996 *Borel-Laplace Transform and Asymptotic Theory* (Boca Raton, FL: CRC Press)
[30] Berry M V and Mount K E 1972 *Rep. Prog. Phys.* **35** 315
[31] Adachi S 1989 *Ann. Phys., NY* **195** 45
[32] Shudo A and Ikeda K S 1996 *Phys. Rev. Lett.* **76** 4151
[33] Doll J D, George T G and Miller W H 1973 *J. Chem. Phys.* **58** 1343
[34] Brink D M and Smilansky U 1983 *Nucl. Phys.* A **405** 301
[35] Wiggins S 1990 *Introduction to Applied Nonlinear Dynamical Systems and Chaos* (New York: Springer)
[36] Takahashi K and Ikeda K S in preparation
[37] Davis M J and Gray S K 1986 *J. Chem. Phys.* **84** 5389
[38] Wiggins S, Weisenfeld L, Jaffe C and Uzer T 2001 *Phys. Rev. Lett.* **86** 5478
[39] Greene J M and Percival I C 1981 *Physica* D **3** 530
Percival I C 1982 *Physica* D **6** 67